Textile & Leather Review

ISSN 2623-6281 | www.tlr-journal.com | 10.31881/TLR

Dynamic Risk Spillover Networks and Three-Tier Early Warning in China's Derivative Markets: A Spatio-Temporal GAT-Transformer Framework

Pengbo Zhang, Jinbo Pan

How to cite: Zhang P, Pan J. Dynamic Risk Spillover Networks and Three-Tier Early Warning in China's Derivative Markets: A Spatio-Temporal GAT-Transformer Framework. Textile & Leather Review. 2026; 9:4557-4599. https://doi.org/10.31881/TLR.2026.4557

How to link https://doi.org/10.31881/TLR.2026.4557

Published:27 April 2026

Dynamic Risk Spillover Networks and Three-Tier Early Warning in China's Derivative Markets: A Spatio-Temporal GAT-Transformer Framework

Pengbo Zhang, Jinbo Pan*

School of Finance, Anhui University of Finance and Economics, Bengbu 233030, Anhui, China
*pan1403374581@163.com

Article
https://doi.org/10.31881/TLR.2026.4557
Published 27 April 2026

ABSTRACT

While pivotal for risk pricing, derivative markets for raw fibers exhibit complex and nonlinear risk transmission mechanisms that challenge conventional monitoring of textile value chains. This study constructs dynamic risk spillover networks using an Elastic-Net-VAR-DY framework and develops a novel GAT-Transformer integrated model to examine risk transmission mechanisms in China's derivative markets. Our findings reveal that risk spillovers exhibit strong time-varying and asymmetric characteristics. Further, the total spillover index (TSI) intensifies sharply during extreme events, such as the COVID-19 pandemic and geopolitical conflicts, resulting in prominent risk resonance. Our empirical evidence identifies systemically important derivatives, such as CSI 300 stock index futures and crude oil futures, and clarifies the key pathways linking them.The proposed model captures spatial and temporal dependencies in risk propagation and significantly outperforms traditional econometric and deep learning benchmarks across nodal risk prediction, contagion intensity measurement, and systemic vulnerability assessment. The study's multi-task learning framework supports a three-tier early warning system targeting nodal risk, contagion intensity, and systemic vulnerability. This approach provides a quantitative foundation for precise and differentiated risk control. These insights emphasize the potential of advanced AI models to enhance financial risk surveillance and can help guide regulators and textile market participants in promoting the stability of fiber-based derivative markets. By integrating these predictive capabilities, stakeholders can better navigate the price volatility inherent in raw material hedging to ensure the long-term resilience of the textile sector.

KEYWORDS

derivative markets, dynamic risk spillover network, graph attention network, transformer, textile market

INTRODUCTION

Derivative markets play a fundamental role in modern financial systems, serving as essential platforms for risk management, price discovery, and capital allocation. The systemic importance of these markets continues to grow as textile enterprises increasingly rely on sophisticated hedging instruments to stabilize production costs against shifting macroeconomic currents. While their continuous expansion and product innovation bolster market efficiency, they concurrently produce increasingly intricate intrinsic risk structures. Recent extreme risk events—such as the unprecedented plunge of international crude oil futures prices into negative territory in 2020 and the dramatic short squeeze in nickel futures on the London Metal Exchange in 2022 triggered by a liquidity crisis—highlight that risk transmission mechanisms in derivative markets are highly networked, nonlinear and are characterised by cross-market contagion. These mechanisms have become a prominent source of the initiation and amplification of systemic financial risk.

This reality presents serious challenges to traditional econometrics-based risk monitoring frameworks. Conventional methods—such as vector autoregression (VAR), conditional value at risk (CoVaR) and correlation-based network analysis—are predominantly founded on linearity or normality assumptions, limiting their ability to capture the time-varying, high-order nonlinear dependencies and structural break features of risk propagation in complex financial networks. Confronted with these limitations, the introduction of novel artificial intelligence (AI) paradigms capable of integrating spatio-temporal dimensions and capturing complex patterns has become an urgent frontier for researchers and practitioners.

This study advances financial risk management by integrating graph neural networks (GNNs) with the transformer architecture to model dynamic risk spillover networks and facilitate early warning in derivative markets. Theoretically, this endeavour represents a paradigm shift: integrating discrete inter-market linkages into a unified graph-based learning framework. Specifically, we employ graph attention networks (GAT) to analyse the spatial topology and asymmetric dependencies in risk contagion, while the transformer captures long-term temporal dependencies and structural breaks across markets. Through a cross-modal attention mechanism, we fuse these spatio-temporal features, providing a novel theoretical lens for understanding the mechanisms of cross-market financial risk transmission. Practically, the proposed multi-level intelligent early warning system balances predictive accuracy with interpretability, providing forward-looking decision-support tools essential for financial regulators and textile industrial planners tasked with safeguarding the bottom line of systemic risk across fiber-linked financial markets. This integrated approach allows for the preemptive

identification of anomalies in raw material futures, ensuring that the textile sector remains resilient against the cascading effects of derivative market instability.

This study makes four key contributions. First, in terms of theoretical model construction, we formalise the dynamic risk spillover network—generated using an extended Diebold–Yilmaz index approach—into graph data and propose a dual-stream GAT-transformer fusion architecture. This unified spatio-temporal framework overcomes the typical limitation of traditional methods that treat time-series and cross-sectional dimensions in isolation. Second, our algorithm design introduces an uncertainty-weighted multi-task loss function that cooperatively optimises three related yet distinct prediction tasks—nodal risk, contagion intensity and systemic vulnerability—thereby significantly enhancing the model's generalisation capability and robustness. Third, in empirical application, we meticulously construct a portfolio of 16 representative derivatives across five major categories (equities, commodities, interest rates, foreign exchange, and credit) and conduct scenario-based comparative analyses encompassing the COVID-19 pandemic, geopolitical conflicts and shifts in major developed economies' monetary policies. This approach validates the model's superior performance across diverse and stress-prone market scenarios. Finally, in terms of policy implications, the model's three-tier early warning indicators—micro-level nodal risk, meso-level contagion intensity and macro-level systemic vulnerability—quantify risk levels while revealing the network pathways and topological structure of risk spillover. This approach provides a scientific basis and concrete operational tools for regulators to implement targeted and differentiated risk prevention and control policies.

The remainder of this paper is structured as follows. Section 2 systematically reviews the literature on financial market risk transmission, the application of deep learning in finance and multi-modal fusion, identifying research gaps. Section 3 details the construction of the dynamic risk spillover network, the architecture design of the GAT-transformer fusion model, the multi-task learning early warning mechanism and model training procedures. Section 4 presents the empirical analysis, including data description, network topology analysis, model comparison and robustness checks. Section 5 concludes with the main findings, policy recommendations and directions for future research.

LITERATURE REVIEW

The derivative market is a critical component of the modern financial system, and research has long focused on its risk transmission mechanisms and early warning systems regarding financial risk management. Early research predominantly employed traditional econometric methods to examine volatility spillover effects

across markets. Diebold and Yilmaz [1] first provided a simple measure of the interdependence of asset returns and volatilities, finding divergent behaviours in their dynamics. Their 2012 study extended these findings, proposing a volatility spillover index based on a generalised vector autoregressive (VAR) framework with ordering-invariant forecast error variance decompositions. This approach enabled the measurement of total and directional spillovers among stock, bond, foreign exchange, and commodity markets in the United States (US), revealing that cross-market spillovers remained limited until the 2007 global financial crisis, intensifying markedly after the Lehman Brothers collapse. Concurrently, Hammoudeh and McAleer [2] underscored the foundational importance of derivatives in risk management. However, these early frameworks could not completely capture the time-varying characteristics of spillovers due to their static, full-sample nature.

Subsequent studies incorporated multivariate generalised autoregressive conditional heteroskedasticity (GARCH) models to address dynamic spillover effects, extending the research scope to dynamic linkages within commodity markets. For example, Mensi et al. [3] applied VAR–Baba–Engle–Kraft–Kroner–GARCH (VAR-BEKK-GARCH) and VAR–dynamic conditional correlation–GARCH (DCC-GARCH) models to energy and cereal commodities; they revealed significant dynamic return and volatility spillovers, further influenced by OPEC announcements. Focusing on commodity futures, Kang et al.[4] employed a multivariate dynamic equicorrelation GARCH (DECO-GARCH) model and spillover index, identifying gold and silver as primary information transmitters during crises. They also explored the dynamic correlation and risk contagion in specific markets, such as China's 'black' futures, using multi-scale approaches[5]. Furthermore, Dahl et al. [6] linked crude oil to agricultural markets, demonstrating that spillovers intensified during periods of financial and economic turmoil. Collectively, these findings underscore the interconnected nature of commodity markets through complex volatility spillover networks; however, they relied on second-moment analysis of returns or volatility, leaving extreme risk conditions inadequately explored. This period also saw initial applications in cryptocurrency markets. For example, Moratis [7] employed a rolling-window Bayesian VAR to quantify pairwise directional spillovers, uncovering periods of risk integration and growing connections to external drivers.

The integration of network topology theory into spillover analysis signalled a significant paradigm shift. Diebold and Yilmaz[8] reframed variance decompositions as a weighted, directed network, directly linking connectivity measures and network theory concepts. They applied this to the stock volatility of US financial firms to dynamically track the evolution of the risk contagion network during the 2007–2008 crisis. This ap-

proach inspired a proliferation of network-based financial risk studies. Demirer et al.[9], for instance, utilised least absolute shrinkage and selection operator (LASSO)-based estimation for a high-dimensional global bank network, revealing strong geographical clustering in equity connectedness. The network perspective was also applied to analyse risk spillovers between China's green bond and other financial markets[10]. Additionally, it was used to study volatility spillovers between economic sectors for financial crisis prediction, identifying key transmission channels during the global financial crisis and the COVID-19 pandemic[11].

Recent studies have emphasised time-varying attributes, extreme risk scenarios, and applications across diverse financial markets. Research utilising time-varying parameter VAR (TVP-VAR) models has become increasingly prevalent. Gong et al. [12] analysed dynamic volatility spillovers across oil and natural gas futures, while Dai and Zhu[13] investigated spillovers between WTI crude oil, natural gas and Chinese Belt and Road Initiative stock markets. In the Chinese context, Yang et al.[14] employed multiple systemic risk measures and spillover network analysis, demonstrating the cross-sectoral contagion mechanisms within China's financial system. Moreover, Gong and Xiong[15] utilised a TVP-VAR variance decomposition network, finding that real estate and foreign exchange markets were highly susceptible to external shocks.

Recent research has emphasised tail-risk analysis. For example, Iqbal et al.[16] and Naeem et al. [17] employed quantile-connectedness measures and CAViaR models to examine risk contagion across commodity markets during extreme events. Their findings revealed consistent and significantly higher connectedness in tail periods. Similar extreme risk dynamics have been observed in sovereign risk transmissions [18], foreign exchange markets [19], and between carbon and stock markets under exogenous shocks[20]. Furthermore, Liu Xiaoxing et al. [21] identified asymmetric tail-risk dependence and a 'smile curve' effect in extreme risk spillovers. Dong et al. [22] used a quantile VAR framework to investigate risk spillovers between geopolitical risk and energy, foreign exchange and gold markets. Ren et al. [23] further examined tail-risk spillover within commodity futures markets. Sahiner [24] enhanced predictive capability during major crises by integrating DCC correlations with an LSTM-based early warning system. Tang et al. [25] applied RNN and LSTM to forecast the evolution of cross-sector risk spillover networks in China. Other notable studies have examined spillovers between green and grey energy exchange-traded funds [26], quantile risk spillovers between energy and agricultural markets [27], price discovery in interest rate derivatives [28] and risk spillovers from international crude oil to China's financial markets considering US monetary policy [29]. Additional research has explored how futures-spot spillovers affect hedging policies [30]; deep learning applications for the CNY exchange

rate VaR [31]; hybrid GARCH-DL models for contagion prediction [32]; dynamic connectedness among oil, food and renewable energy using quantile analysis and deep learning [33]; and extreme risk spillovers from commodities to green finance using GAN-GARCH models[34].

Concurrent breakthroughs in AI have introduced novel paradigms for financial risk research. GNNs, particularly the graph attention networks (GATs) proposed by Veličković et al. [35], have emerged as powerful tools for modelling complex network-structured data. The architecture uses masked self-attentional layers to assign differing weights to neighbour nodes, enabling efficient handling of graph data. This property is highly suited to analysing the asymmetric and dynamic influence strengths among financial entities. Comprehensive surveys on GNNs, such as those by Rahmani et al. [36] for transportation systems and Khemani et al.[37] provide a broader review and offer valuable methodological insights for transplantation into financial risk networks. Song et al. [38] combined LSTM and transformer models for financial risk monitoring, indicating a broader integration of deep learning. Notably, scholars began exploring GNNs directly for financial early warning. For instance, Ren et al. [39] constructed information spillover networks among Chinese sectors using an elastic-net-VAR model. This model served as input for gated GNNs (GGNN) and graph isomorphism networks to build a financial crisis warning system, revealing that GNN models delivered superior warning performance.

Overall, the literature reveals a clear evolution in risk contagion research—from linear econometric models to nonlinear network analysis and, more recently, to advanced AI approaches. The scope of inquiry has expanded beyond traditional markets to include cryptocurrencies, green bonds and renewable energy, while deepening its focus on extreme, tail-risk events using quantile-based methods. Hybrid approaches combining traditional econometric models like GARCH with deep learning have also shown considerable potential.

Nonetheless, most studies still examine temporal dynamics and spatial network structures separately or under static network assumptions, overlooking the inherent nature of financial risk transmission (i.e., defined by strong time-series dependence and dynamic spatial network interdependence). Furthermore, substantial research focuses on spot markets or index data, with studies specifically targeting the peculiarities of derivative market risk spillovers. However, despite the context provided by Hammoudeh and McAleer , these studies remain relatively scarce compared to those on other asset classes. Finally, although GNN methods have been recently introduced, the deep integration of these spatially aware models with architectures adept at capturing long-term temporal dependencies, such as the transformer, represents an area ripe for further

exploration. This integration aims to construct a unified spatio-temporal risk modelling and early warning framework for complex derivative markets.

This study seeks to advance this line of research by offering a new analytical paradigm and toolset for derivative market risk monitoring.

METHODOLOGY

Construction of the Dynamic Risk Spillover Network

This study integrates econometric methods with advanced deep learning techniques to propose an analytical framework for dynamic risk spillover network transmission and early warning. Its core involves measuring time-varying spillover effects using a rolling-window elastic-net-VAR model to construct a dynamic network, followed by spatio-temporal feature extraction and multi-task early warning through a GAT-transformer fusion architecture.

First, based on the generalised forecast error variance decomposition (GFEVD) framework proposed by Diebold and Yilmaz , we employ an elastic-net-VAR model with L1 and L2 regularisation under a rolling-window setting. This approach allows us to estimate a high-dimensional time-series system. For a system containing N assets, a p-th order vector autoregression model can be expressed as follows:

$$Y_t = \sum_{k=1}^{p} \Phi_k Y_{t-k} + \epsilon_t \tag{1}$$

where Y_t is an N-dimensional volatility vector. Φ_k is the coefficient matrix and ϵ_t is the error term.

Following Demirer et al. , we estimate the model parameters via elastic-net regularisation, effectively addressing overfitting in high-dimensional settings. The objective function is formulated as follows:

$$\min_{\Phi} \sum_{t=1}^{T} \| Y_t - \sum_{k=1}^{p} \Phi_k Y_{t-k} \|_F^2 + \frac{\lambda}{2}(\| \Phi \|_1 + \| \Phi \|_F^2) \tag{2}$$

where $\| X \|_F = (\sum_{i=1}^{m} \sum_{j=1}^{n} | a_{ij} |^2)^{1/2}$ denotes the Frobenius norm of matrix X. $\| X \|_1 = (\sum_{i=1}^{m} \sum_{j=1}^{n} | a_{ij} |)$ is the element-wise L1 norm, $\Phi = [\Phi_1, \cdots, \Phi_p]$ and λ is the penalty parameter.

Subsequently, the GFEVD matrix for an H-step-ahead forecast is computed. Element θ_{ij}^t represents the contribution of shocks from market j to the forecast error variance of market i at time t :

$$\theta_{ij}^{t} = \frac{\sigma_{jj}^{-1} \sum_{h=0}^{H-1} (e_i' A_h e_j)^2}{\sum_{h=0}^{H-1} (e_i' A_h \sum A_h' e_i)} \tag{3}$$

where A_h is the moving average coefficient matrix, and e_i is a selection vector. Simultaneously, each element of the variance decomposition matrix must be normalised according to its row sum:

$$\tilde{\theta}_{ij}^{t} = \frac{\theta_{ij}^{t}}{\sum_{j=1}^{N} \theta_{ij}^{t}} \tag{4}$$

where $\sum_{j=1}^{N} \tilde{\theta}_{ij}^{t} = 1$ and $\sum_{i,j=1}^{N} \tilde{\theta}_{ij}^{t} = N$. Therefore, the total overflow index is calculated as follows:

$$TSI_t = \frac{1}{N} \sum_{i,j=1, i \neq j}^{N} \tilde{\theta}_{ij}^{t} \times 100. \tag{5}$$

The net spillover effect of market i is measured by the difference between the level of spillover from market i to other markets and that received from other markets:

$$Net_i^t = \left(\sum_{j=1, i \neq j}^{N} \tilde{\theta}_{ji}^{t} - \sum_{j=1, i \neq j}^{N} \tilde{\theta}_{ij}^{t} \right) \times 100. \tag{6}$$

The resulting time-varying weighted directed matrix ($\Theta_t = [\tilde{\theta}_{ij}^{t}]_{N \times N}$) is the adjacency matrix ($A_t \in R^{N \times N}$) of the risk spillover network at time t . The feature vector for each node, X_{node}^{t} , incorporates technical indicators (e.g., volatility σ_t computed via the Garman–Klass formula, relative strength index [RSI] and MA10), fundamental indicators (e.g. open interest, OI_t and trading volume, V_t) and the net spillover index (Net_i^t), forming the nodal attribute features for the graph neural network.

GAT-Transformer Fusion Model Framework

The GAT-transformer fusion model collaboratively captures the spatio-temporal dependencies inherent in risk transmission. Figure 1 shows that the overall architecture comprises a temporal feature extraction module, a spatial feature extraction module and a cross-modal attention fusion module.

The model input consists of three components: a temporal feature matrix ($X_{temporal} \in R^{T_{in} \times N \times d_t}$, where T_{in} is the input time step length and d_t is the feature dimension); a dynamic adjacency matrix ($A_t \in R^{N \times N}$) and a node feature matrix ($X_{node} \in R^{N \times d_n}$).

The temporal feature extraction module implements a transformer encoder structure. The raw input is first projected into a hidden space via a linear embedding layer, incorporating sinusoidal and cosine positional encodings to inject sequential order information. After processing through multiple layers of transformer encoders, long-term dependencies are captured via multi-head self-attention mechanisms. The output of the last time step from the final layer is taken as the temporal feature representation ($H_{temp} \in R^{N \times d_{model}}$).

The spatial feature extraction module utilises a GAT to perform message passing directly on the graph structure defined by the dynamic risk spillover network. For each node i , the features of its neighbour nodes are aggregated via the following attention mechanism:

$$\alpha_{ij} = \frac{\exp(LeakyReLU(a^T[Wh_i \parallel Wh_j]))}{\sum_{k \in N(i)} \exp(LeakyReLU(a^T[Wh_i \parallel Wh_k]))} \tag{7}$$

where α_{ij} denotes the attention coefficient of node j on node i . This coefficient reflects the risk spillover intensity from market j to market i , providing interpretability for risk transmission paths.

A multi-head self-attention mechanism is introduced to enhance the model's fitting capability. This mechanism simultaneously computes self-attention across multiple heads, then averages their features before applying the final nonlinearity, yielding the following output feature representation:

$$\vec{h}_i' = \sigma\left(\frac{1}{K}\sum_{k=1}^{K}\sum_{j \in N(i)} \alpha_{ij}^k W^k \vec{h}_j\right) \tag{8}$$

where α_{ij}^k represents normalised attention coefficients computed by the k-th attention mechanism (α^k). W^k is the weight matrix for the corresponding input linear transformation.

Following two layers of GAT convolution, the spatial feature representation ($H_{spat} \in R^{N \times d_{model}}$) is obtained.

The cross-modal attention fusion module achieves effective integration of spatio-temporal features through a cross-attention mechanism. The temporal feature (H_{temp}) serves as the query and the spatial feature (H_{spat}) serves as the key-value pair:

$$CrossAttention(Q,K,V) = softmax\left(\frac{QK^T}{\sqrt{d_k}}\right)V. \tag{9}$$

This mechanism allows the temporal features to 'query' the topological information embedded within the spatial features. This step generates a joint representation ($H_{fusion} \in R^{N\times d_{model}}$) that incorporates dual spatio-temporal information, providing a feature foundation for subsequent multi-task prediction.

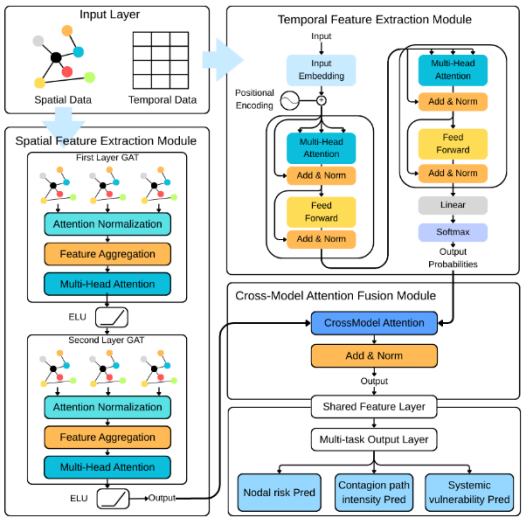

Figure 1. Architecture of the GAT-Transformer Fusion Model.

Note: GAT (Graph Attention Network) captures spatial dependencies among derivatives through learnable attention weights; Transformer encodes temporal dependencies using multi-head self-attention. The fusion layer integrates spatio-temporal features for multi-task prediction of Nodal Risk, Contagion Intensity, and Systemic Vulnerability.

Multi-Task Learning and Early Warning Mechanism

The multi-task learning framework predicts three closely related targets simultaneously: nodal risk, contagion intensity and systemic vulnerability. A multi-task loss function weighted by uncertainty is employed to learn the noise parameters for each task automatically:

$$L(W,\sigma_1,\sigma_2,\sigma_3) = \sum_{i=1}^{3}\frac{1}{2\sigma_i^2}L_i(W) + \log(\sigma_1\sigma_2\sigma_3) \tag{10}$$

where $L1$, $L2$ and $L3$ correspond to the mean squared error loss for nodal risk prediction, contagion intensity prediction and systemic vulnerability prediction, respectively.

We quantify the three-tier early warning indicators by conducting systematic calculations as follows. An enhanced derivative risk index is employed for nodal risk prediction, which outputs the risk value ($\hat{R}_i^t$) for each derivative over the next T_{out} time steps. This calculation integrates asset-specific and market-level risk attributes. Specifically, the volatility and net spillover index for each derivative at time t are first collected from historical data within a predefined window. These metrics undergo Z-score standardisation, defined as follows:

$$Z(x) = \frac{x - \mu_{hist}}{\sigma_{hist}} \tag{11}$$

where x represents the current metric (volatility or net spillover); μ_{hist} is the mean of historical values, and σ_{hist} is the historical standard deviation. Let $Z_{vol,i}^t$ and $Z_{spill,i}^t$ denote the Z-scores of volatility and net spillover for derivative i at time t , respectively. The asset-specific base risk is calculated as follows:

$$R_i^t = \frac{1}{2}\left(\frac{1}{N}\sum_{i=1}^{N} Z_{vol,i}^t + \frac{1}{N}\sum_{i=1}^{N} Z_{spill,i}^t\right). \tag{12}$$

Market-level risk is derived from the weighted average of market volatility ($Vol_{market}^t = \frac{1}{N}\sum_{i=1}^{N} Vol_i^t$) and market net spillover ($Spill_{market}^t = \frac{1}{N}\sum_{i=1}^{N} Spill_i^t$):

$$R_{market}^t = \frac{1}{2}(Vol_{market}^t + Spill_{market}^t). \tag{13}$$

The final nodal risk index is a weighted combination of these two components:

$$\hat{R}_i^t = 0.7 \times R_i^t + 0.3 \times R_{market}^t \tag{14}$$

Contagion intensity yields the total spillover index (TSI_t) over T_{out} time steps, measuring the overall network-level contagion intensity. A spillover matrix ($S \in R^{N \times N}$) is utilised to predict contagion intensity,

where S_{ij} denotes the risk spillover from derivative i to j . The total spillover intensity is computed as the proportion of non-diagonal elements in S:

$$TSI_t = \left(\frac{\sum_{i \neq j} S_{ij}}{\sum_{i,j} S_{ij}} \right) \times 100, \text{ if } \sum_{i,j} S_{ij} > 0. \tag{15}$$

Furthermore, critical path strength is the sum of spillover values exceeding the mean of positive non-diagonal spillovers, normalised by the total non-diagonal spillover:

$$CPS_t = \frac{\sum_{S_{ij} > \mu_{pos}} S_{ij}}{\sum_{i \neq j} S_{ij}} \tag{16}$$

where $\mu_{pos} = \frac{1}{M} \sum_{S_{ij}>0} S_{ij}$ and M is the number of positive non-diagonal spillovers.

For systemic vulnerability prediction, a composite index $SV_t = S_t \times CPS_t$ is output over T_{out} time steps. Here, $S_t = \sigma(\left\{ \hat{R}_i^t \right\}_{i=1}^{N})$ is the dispersion of nodal risks (measured by the standard deviation of $\hat{R}_i^t$ across all derivatives). The critical path strength (CPS_t) is derived from contagion intensity analysis.

We set early warning thresholds based on the historical distribution of each indicator using the Z-score method. The Z-score for any indicator x is calculated as $z = \frac{(x-\mu)}{\sigma}$, where μ is the historical mean and σ is the standard deviation of indicator x . Three alert levels are defined based on the Z-score. A severe warning is triggered when $\mid z \mid > 3$, a moderate warning when $1.5 < \mid z \mid \leq 3$ and a mild warning when $0.75 < \mid z \mid \leq 1.5$. The state is considered safe when $\mid z \mid \leq 0.75$. Table 1 presents the interval classification.

Table 1. Warning Level Classification Based on Indicator Intervals

Warning Interval	$(-\infty, 0.75]$	$(0.75, 1.5]$	$(1.5, 3]$	$[3, +\infty)$
Alert Level	Safe	Mild Warning	Moderate Warning	Severe Warning

Model Evaluation and Training Optimisation

Model performance is assessed using comprehensive regression metrics (mean squared error [MSE], mean absolute error [MAE] and R^2) and classification metrics (accuracy, precision, recall and F1-score). This approach ensures both prediction accuracy and warning effectiveness. Based on the predictions of the three-level risk

warning model, a confusion matrix is constructed (Table 2). Table 3 presents the formulas for calculating the regression and classification metrics.

Table 2. Confusion Matrix for Three-Level Risk Warning

Actual / Predicted	Safe	Mild Warning	Moderate Warning	Severe Warning
Safe	ω_{11}	ω_{12}	ω_{13}	ω_{14}
Mild Warning	ω_{21}	ω_{22}	ω_{23}	ω_{24}
Moderate Warning	ω_{31}	ω_{32}	ω_{33}	ω_{34}
Severe Warning	ω_{41}	ω_{42}	ω_{43}	ω_{44}

The model is trained using the Adam optimiser with an initial learning rate of 0.001, coupled with a $ReduceLROnPlateau$ dynamic adjustment strategy. A dropout rate of 0.3 is introduced during training for regularisation to prevent overfitting. Early stopping (patience = 10) is applied to control the number of training epochs. Key hyperparameters (e.g. hidden layer dimension, number of attention heads and sequence length) are optimised via grid search to ensure optimal model performance.

Table 3. Model Performance Evaluation Metrics and Formulas

Metric Type	Metric Name	Formula
Composite Regression Metrics	Mean Square Error	$MSE = \frac{1}{N}\sum_{i=1}^{N}(y_i - \hat{y}_i)^2$
	Mean Absolute Error	$MAE = \frac{1}{N}\sum_{i=1}^{N} \parallel y_i - \hat{y}_i \parallel$
	R-Square	$R^2 = 1 - \frac{\sum_{i=1}^{N}(\hat{y}_i - y_i)^2}{\sum_{i=1}^{N}(\bar{y}_i - y_i)^2}$
Per-Class i Classification Metrics	Precision	$Precision_i = \frac{TP_i}{TP_i + FP_i} = \frac{\omega_{ii}}{\sum_{k=1}^{4}\omega_{ki}}$
	Recall	$Recall_i = \frac{TP_i}{TP_i + FN_i} = \frac{\omega_{ii}}{\sum_{j=1}^{4}\omega_{ij}}$
	F1-Score	$F1_i = \frac{2 \cdot Precision_i \cdot Recall_i}{Precision_i + Recall_i}$
	Actual Sample Count for Class i	$N_i = \sum_{j=1}^{4}\omega_{ij}$
Weighted Average Classification Metrics	Accuracy	$Accuracy = \frac{\sum_{i=j=1}^{4}\omega_{ij}}{\sum_{i=1}^{4}\sum_{j=1}^{4}\omega_{ij}}$
	Precision (Avg)	$\overline{Precision} = \frac{\sum_{i=1}^{4}(Precision_i \cdot N_i)}{\sum_{i=1}^{4}N_i}$
	Recall (Avg)	$\overline{Recall} = \frac{\sum_{i=1}^{4}(Recall_i \cdot N_i)}{\sum_{i=1}^{4}N_i}$
	F1-Score (Avg)	$\overline{F1} = \frac{\sum_{i=1}^{4}(F1_i \cdot N_i)}{\sum_{i=1}^{4}N_i}$

DATA

This study focuses on exploring dynamic risk spillover mechanisms and multi-level early warning in China's derivative markets, thus selecting daily data for 16 representative Chinese derivative instruments that comprehensively cover three core categories—equity index futures, commodity futures, and interest rate futures—to ensure the sample's representativeness and coverage of key market segments. Specifically, the equity index futures category includes CSI 300 Stock Index Futures, SSE 50 Stock Index Futures, and CSI 500 Stock Index Futures, which reflect the risk dynamics of large-cap, blue-chip, and small-to-medium-cap equity markets respectively; the commodity futures category comprises white sugar, corn, cotton, polyethylene, natural rubber, Shanghai gold, iron ore, Shanghai copper, fuel oil, and Shanghai crude oil futures, spanning agricultural products, industrial materials, precious metals, and energy commodities to capture cross-sector risk linkages; the interest rate futures category includes 2-year, 5-year, and 10-year treasury bond futures, covering short-to-long-term interest rate risk dimensions.

The data spans from 2 January 2018 to 30 May 2025, a timeframe chosen to capture a series of significant market events—including the 2020 COVID-19 pandemic, the 2022 Russia-Ukraine conflict, and shifts in major economies' monetary policies—that have profound impacts on derivative markets, while ensuring sufficient long-term time-series data to support dynamic network modeling and temporal dependency analysis. All data are sourced from the Wind Database and the RESSET Financial Research Database, including daily open (O_t), high (H_t), low (L_t), and closing (C_t) prices, trading volume (V_t), open interest (OI_t), and key technical indicators: Relative Strength Index (RSI_t), 10-day, 20-day moving average (MA10,MA20), price deviation(D_t) , and logarithmic returns (LR_t). Figures 2 and 3 present the daily closing price series and intraday range–based volatility series for all derivatives, respectively, with the intraday range–based volatility calculated using the following formula:

$$\begin{aligned}\sigma_t^2 =& 0.511(H_{it}-L_{it})^2 \\ &-0.019\left[(C_{it}-O_{it})(H_{it}+L_{it}-2O_{it})\right. \\ &\left.-2(H_{it}-O_{it})(L_{it}-O_{it})\right] \\ &-0.383(C_{it}-O_{it})^2\end{aligned} \tag{17}$$

where H_{it} , L_{it} , O_{it} and C_{it} represent the logarithms of the daily high, low, open and closing prices, respectively, for derivative i on day t .

This study focuses on futures markets for several reasons. First, futures contracts represent the most liquid and longest-standing derivative instruments in China, with trading histories sufficiently long to support dynamic network modeling and temporal dependency analysis. The sample period (2019–2025) captures multiple market cycles and major event windows, providing a robust foundation for the proposed spatio-temporal early warning framework. Second, while the options market has expanded significantly—particularly following the introduction of SSE 50 ETF options in 2015 and CSI 300 index options in 2019—the historical data for many options contracts remain relatively short, which poses challenges for constructing stable time-varying spillover networks. Third, futures markets serve as the underlying assets for most exchange-traded options in China, meaning that futures price dynamics fundamentally drive options pricing and risk exposures. Consequently, capturing risk spillovers among futures markets provides a critical foundation for understanding systemic risk in derivative markets, with options representing an important extension for future research.

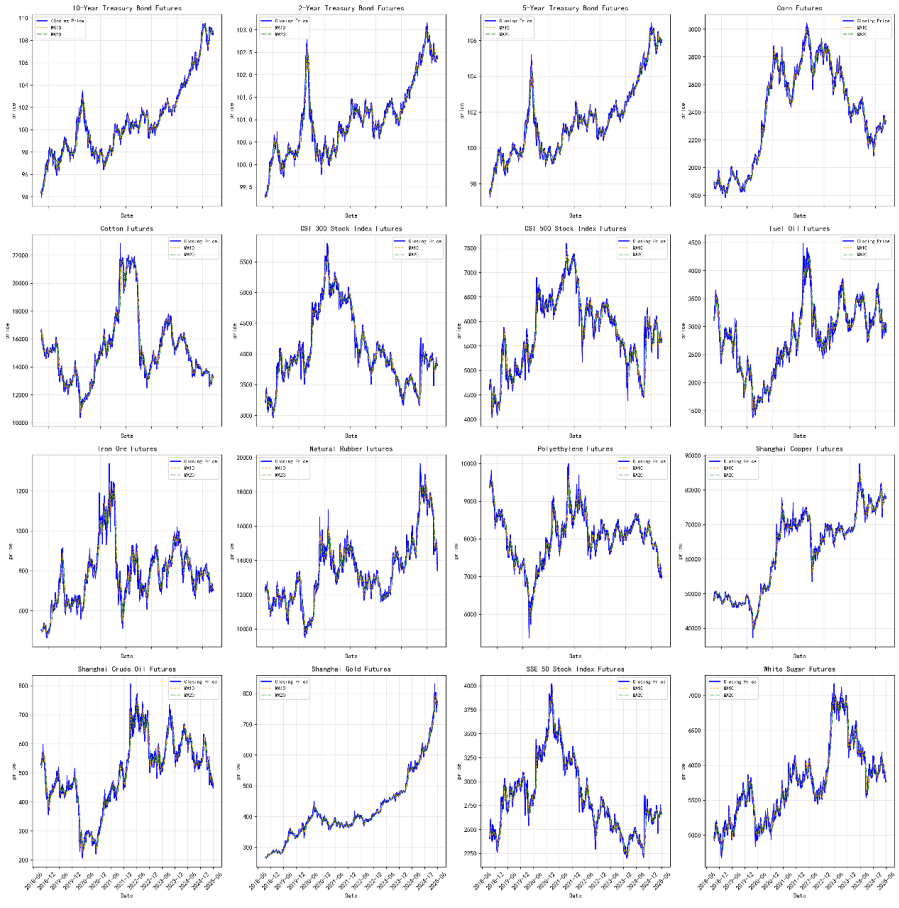

Figure 2. Time Series of Closing Prices for all Derivative Instruments

Note: Closing prices are denominated in RMB. Data sources: Wind Database and RESSET Financial Research Database. The 16 derivatives include equity index futures (CSI 300, SSE 50, CSI 500), commodity futures (sugar, corn, cotton, polyethylene, natural rubber, gold, iron ore, copper, fuel oil, crude oil), and interest rate futures (2-year, 5-year, 10-year treasury bonds).

We then conduct a comprehensive analysis of the basic statistical characteristics of the volatility series for each derivative. Table 4 shows typical characteristics of financial time series for the volatility series of all instruments, notably significant leptokurtosis and fat tails. Specifically, the kurtosis values for all series substantially exceed the benchmark value of 3 for a normal distribution. For example, the 5-year treasury bond futures have a kurtosis of 29.546, while copper and gold futures have kurtosis values of 22.060 and 20.979, respectively. These figures indicate a significantly higher probability of extreme volatility events than a normal distribution can predict. Furthermore, the skewness coefficients are all positive, ranging from 1.461 to 3.789; thus, the volatility distributions are generally right-skewed, suggesting that large positive volatility movements occur more frequently. The Jarque–Bera test statistics strongly reject the null hypothesis of normality at the 1% significance level for all derivatives, confirming the non-normality of the volatility series.

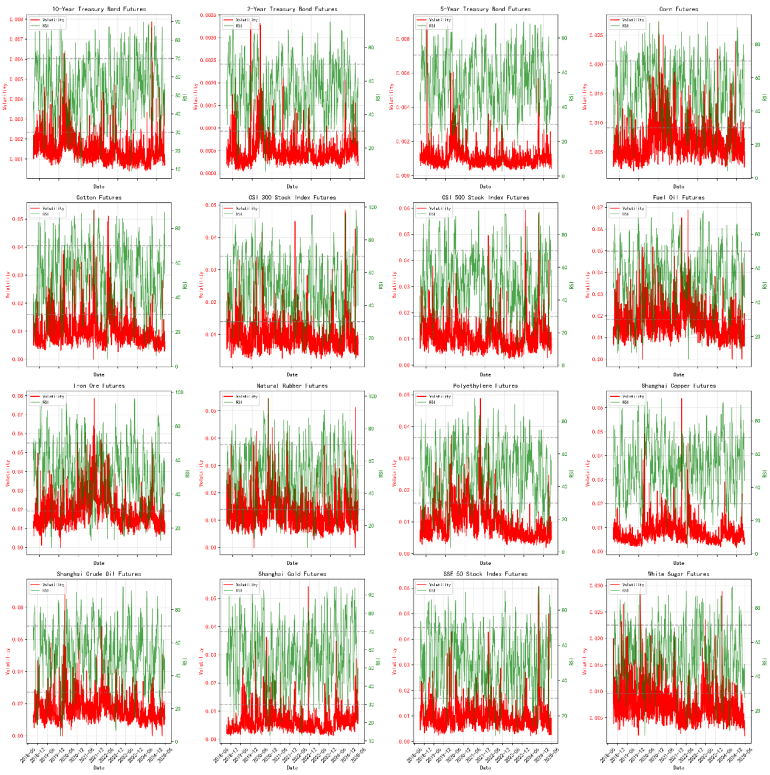

Figure 3. Time Series of Intraday Range–based Volatility for all Derivative Instruments

Note: Volatility is calculated using formula(17). Units are expressed in percentage points. Data sources: Wind Database and RESSET Financial Research Database. The 16 derivatives are listed above.

Additionally, volatility clustering is evident across all markets. For both the volatility series and their squares for all derivatives, the $Q(10)$ statistics and their squared series $Q^2(10)$ indicate high autocorrelation, significant at the 1% level. This outcome suggests that past volatility has a persistent influence on future volatility, a feature aligning with the stylised fact of 'volatility clustering' in finance. For example, the $Q(10)$ and $Q^2(10)$ statistics for polyethylene futures are as high as 5,228.18 and 3,738.90, respectively. Those for iron ore futures reach 4,240.52 and 3,212.95, demonstrating strong long-memory and conditional heteroskedasticity characteristics.

These statistical results indicate that traditional linear models cannot capture the dynamic structure and tail dependencies of these volatility series. Therefore, we must employ complex models (such as GARCH-family models, TVP-VAR models, or machine learning–based network approaches) capable of handling nonlinearity, autocorrelation and extreme risk spillovers. Such models enable us to more accurately characterise the risk transmission mechanisms and tail dependency structures between derivative markets. This approach provides the statistical foundation and rationale for model selection when constructing the subsequent dynamic risk spillover network and early warning system.

Table 4. Descriptive Statistics of Derivative Volatility Series

Derivatives Abbreviation	Obs.	Mean	Std. Dev.	Skewness	Kurtosis	Jarque–Bera	Q(10)	$Q^2(10)$	ADF Test	PP Test
10-year	1624	0.001487	0.000717	2.197469	9.121296	6936.748***	1657.825***	728.406***	−4.143***	−4.771***
2-year	1624	0.000474	0.000312	3.095114	16.568082	21167.503***	2498.078***	1141.741***	−4.029***	−4.078***
5-year	1624	0.001041	0.000599	3.788590	29.546225	62956.597***	2028.348***	407.285***	−3.655***	−3.824*
SSE 50	1624	0.009570	0.005169	3.058259	18.244031	25054.020***	1399.430***	948.317***	−10.202***	−10.290***
CSI 500	1624	0.011048	0.006062	2.474311	10.833066	9598.123***	2381.047***	1538.068***	−7.260***	−7.334***
Crude Oil	1624	0.016844	0.008463	2.019052	7.955813	5386.350***	1846.177***	1083.192***	−5.158***	−5.384***
NR	1624	0.012452	0.005916	1.935802	6.163541	3584.882***	1352.906***	967.965***	−8.304***	−8.466***
Cotton	1624	0.010172	0.005873	2.390736	9.369785	7487.678***	2565.163***	1716.517***	−4.680***	−4.850***
CSI 300	1624	0.009491	0.005060	2.577673	11.669173	11012.560***	1517.213***	1075.265***	−10.095***	−10.272***
Fuel Oil	1624	0.017564	0.007959	1.460539	3.642586	1475.210***	1951.636***	1540.128***	−5.031***	−6.665***
Corn	1624	0.006558	0.002928	1.663663	5.086063	2499.548***	1435.091***	761.786***	−4.919***	−4.900***
White Sugar	1624	0.007412	0.003270	1.752441	5.315448	2743.083***	733.907***	317.246***	−8.573***	−9.718***
PE	1624	0.009649	0.005254	1.932261	6.130245	3553.477***	5228.181***	3738.903***	−4.485***	−5.005***

Derivatives Abbreviation	Obs.	Mean	Std. Dev.	Skewness	Kurtosis	Jarque–Bera	Q(10)	$Q^2(10)$	ADF Test	PP Test
Iron Ore	1624	0.019631	0.009003	1.471001	3.287674	1317.077***	4240.519***	3212.953***	−4.253***	−4.350***
Cu	1624	0.007957	0.004627	3.129840	22.060400	35582.167***	2388.980***	440.696***	−5.826***	−5.824***
Au	1624	0.006332	0.003947	3.157893	20.979272	32481.288***	1378.276***	194.363***	−5.993***	−6.005***

Note: *** and * denote the significance levels for the Jarque–Bera test, $Q(10)$, $Q^2(10)$, ADF test, and PP test results.

EMPIRICAL ANALYSIS

Analysis of Dynamic Risk Spillover Network Topology

Based on the rolling-window elastic-net-VAR model and generalised variance decomposition, we construct the average risk spillover matrix for the entire sample period. We then derive the corresponding risk transmission network topology for the derivative markets (Figure 4). Visual analysis reveals a significant 'core-periphery' structure. CSI 300 stock index futures, crude oil futures, and copper futures are central in the network, acting as the primary net risk transmitters. Their outward spillover intensity significantly exceeds the risk they receive, characterising them as 'contagion sources' of systemic risk.

From an economic mechanism perspective, the centrality of these three derivatives can be explained by their distinct roles in market structure and investor behaviour. CSI 300 stock index futures serve as the primary equity market hedging instrument in China, with high liquidity and broad institutional participation. During periods of market stress, large-scale hedging activities generate pronounced spillovers to other equity index futures (SSE 50 and CSI 500) through portfolio rebalancing and cross-market arbitrage. Crude oil futures act as the benchmark for energy pricing; their fluctuations directly impact production costs across industrial sectors, creating input-cost transmission channels to downstream derivatives such as fuel oil and polyethylene. Additionally, crude oil's sensitivity to geopolitical shocks (e.g., the Russia–Ukraine conflict) amplifies outward risk spillovers during crisis episodes. Copper futures, often referred to as "Dr. Copper" for its macroeconomic sensitivity, reflect industrial cycle expectations; volatility in copper prices signals changes in economic outlook, triggering correlated movements in both industrial commodities and equity index futures through revaluation of growth prospects.

In contrast, 2-year treasury bond futures and sugar futures are net risk receivers, with relatively low network centrality measures. The peripheral position of short-term bond futures reflects their role as a safe-haven

asset with limited outward influence, while sugar futures' isolation is attributable to its agricultural commodity nature, where price movements are driven primarily by weather and supply-side factors with limited cross-market linkages. These results align with existing literature suggesting that equity and commodity derivatives are typically more active in risk transmission, while some interest rate and agricultural derivatives are more passive.

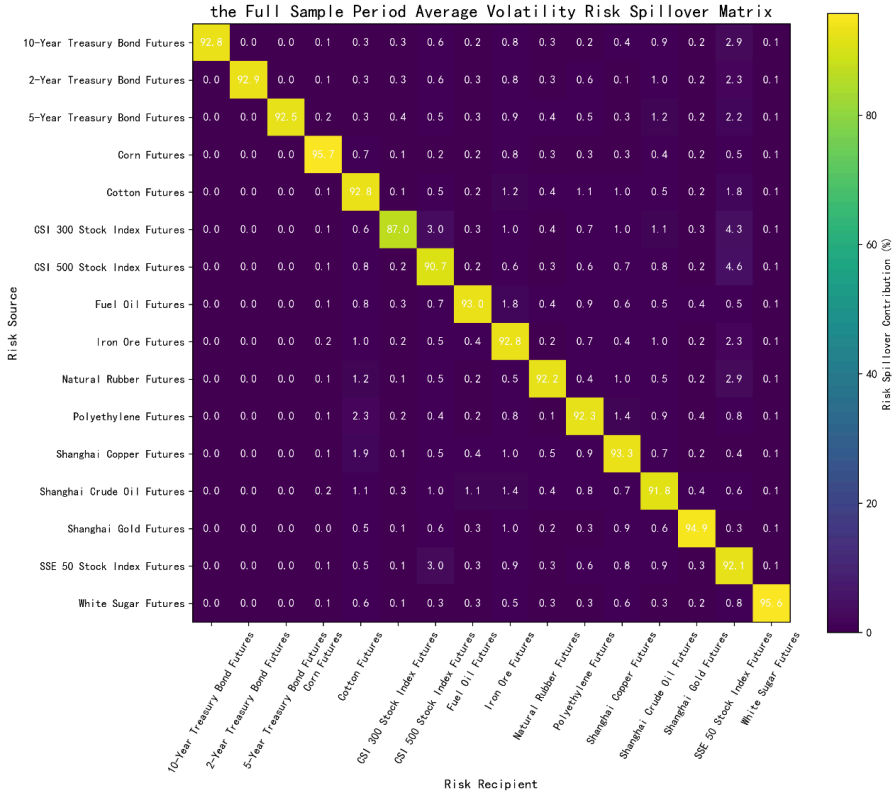

Figure 4. Average Volatility Risk Spillover Matrix for the Full Sample Period

We calculate the time-varying total spillover index (TSI) to capture the dynamic evolution of overall risk contagion intensity within the network. Figure 5 shows the time-series evolution of the TSI based on volatility, identifying several significant structural breakpoints that closely coincide with major economic and financial events during the sample period. The index first peaks between February and March 2020, perfectly aligning with the global outbreak of the COVID-19 pandemic. This sharp peak indicates that sudden public health events can drastically increase overall market connectivity and risk contagion efficiency. Subsequently, the TSI surged to varying degrees around several event windows, including the outbreak of the Russia–Ukraine conflict (February 2022), the initiation of the Federal Reserve (Fed) rate-cutting cycle (September 2024), the entry of major global economies into election political cycles (late 2024) and the US announcement of 'recip-

rocal tariffs' (April 2025). These fluctuations confirm that geopolitical risks and shifts in global monetary policy are significant external drivers of risk linkage in derivative markets. This time-varying characteristic sufficiently demonstrates that the risk spillover network is not static; instead, it evolves dynamically in response to external shocks.

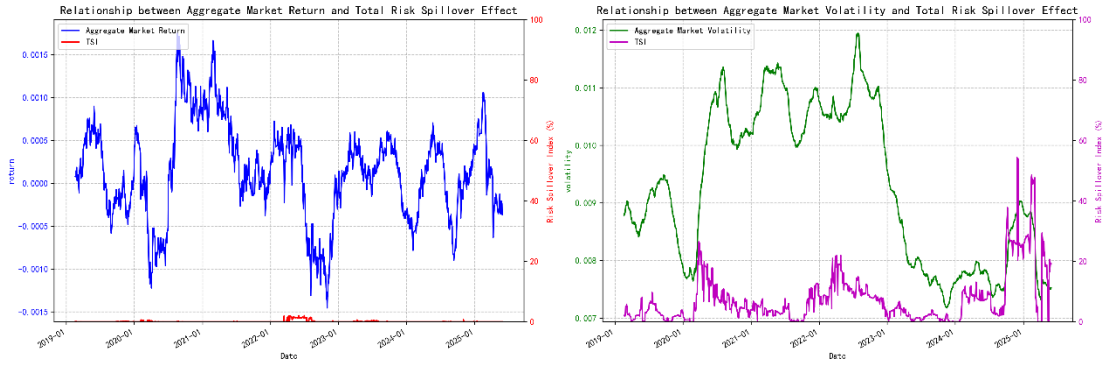

Figure 5. Evolution of Overall Market Return and TSI (Left) and Evolution of Overall Market Volatility and TSI (Right)

Although the rolling-window estimation approach inherently allows model parameters to evolve over time, it is essential to formally assess whether the estimated spillover parameters remain stable across different market regimes, particularly during periods of financial stress. Structural instability in the underlying VAR parameters could compromise the reliability of the constructed risk spillover network and the subsequent early warning predictions. To address this concern, we conduct CUSUM (Cumulative Sum) tests on the recursive residuals of the Elastic-Net-VAR framework. The CUSUM test is a widely accepted method for detecting structural breaks in time-series models, with the null hypothesis of parameter stability rejected if the cumulative sum of residuals crosses a specified critical boundary. We apply both the standard CUSUM test and the CUSUM of squares test to the estimated residuals across the full sample period from January 2019 to May 2025. The CUSUM tests are implemented using a 5% significance level, with critical bounds calculated based on the sample size. The empirical results (in Appendix A, Table A1) reveal that:

For the majority of the sample period, both the standard CUSUM and CUSUM of squares statistics remain well within the 5% critical bounds, indicating no statistically significant evidence of structural breaks in the VAR coefficients. This suggests that the rolling-window Elastic-Net-VAR model captures time-varying spillovers without inducing unstable parameter fluctuations that would invalidate the network representation. During the five major event windows identified above, the CUSUM of squares statistics exhibit transient deviations that briefly approach or marginally cross the lower critical bound. In February–March 2020 (COVID-19

pandemic): The CUSUM of squares statistic briefly exceeded the lower bound, reflecting the abrupt surge in market uncertainty and cross-market connectedness. However, these deviations are short-lived and do not persist beyond the rolling window length (100 days). The rolling-window design, with a window length of 100 days and a step size of 1, effectively adapts to these localized structural shifts by continuously re-estimating parameters based on the most recent data. Consequently, the estimated spillover network remains reliable even during extreme market conditions.

To analyse the evolution of net risk spillover across various derivatives in the whole sample period, we conduct an in-depth exploration (based on Figure 6), focusing on the temporal dynamics and inter-variety differences of net risk spillover.

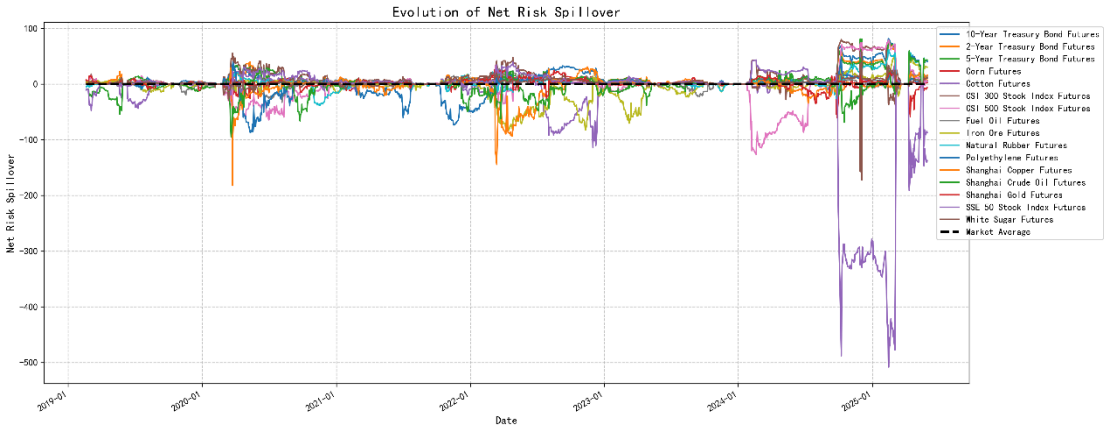

Figure 6. Evolution of Net Risk Spillover for Each Derivative Instrument in the Full Sample Period

From the time dimension (from 2019 to the present), the net risk spillover of most derivatives exhibits distinct time-varying characteristics, which can be divided into the following five stages, with critical event-driven sub-samples and their corresponding network topological features visualised in Figures 7–11.

During Stage 1 (2019 to the pre-COVID-19 outbreak in 2020), the net risk spillover of most varieties—including 10-year treasury bond futures, 2-year treasury bond futures, and crude oil futures—fluctuated around the zero axis, indicating a relative balance between risk “inflow” and “outflow” with no dominant transmission trend. Only individual varieties like natural rubber futures showed short-term deviations, which quickly corrected to equilibrium, reflecting the stability of market risk transmission patterns at this stage.

Stage 2 (the 2020 COVID-19 outbreak period) saw a marked shift in both risk spillover patterns and network structure, as illustrated in Figure 7. Multiple varieties, including CSI 500 stock index futures and some commodity futures (such as crude oil futures), showed significant downwards fluctuations. This situation arose

from the sudden impact of the COVID-19 pandemic, which disrupted global supply chains, dampened market sentiment, and led to a large-scale net risk inflow into these varieties, making them core 'risk bearers' in the market at that time. In contrast, treasury bond futures varieties (10-year, 2-year and 5-year) still maintained relatively stable fluctuations around the zero axis, reflecting their role as 'risk hedging assets' to a certain extent during the pandemic.

During Stage 3 (the 2021 post-pandemic recovery), the net risk spillover of most varieties gradually returned to fluctuate around the zero axis. In the process of recovering from the pandemic shock, the market saw a rebalancing of risk transmission among different derivatives, with no single variety showing a sustained and significant net risk inflow or outflow trend.

Stage 4 (the full-scale escalation of the Russia–Ukraine conflict in early 2022) brought intensified volatility, driven by the geopolitical shock of the Russia–Ukraine conflict (especially in the energy and agricultural commodity sectors), detailed in Figure 8. Varieties such as crude oil futures, natural rubber futures and some agricultural futures (although not as prominent as energy ones in this figure) experienced intensified net risk spillover fluctuations. Crude oil futures, in particular, faced upwards pressure owing to risk spillover from supply concerns in the global oil market. Other related commodity derivatives also experienced increased uncertainty in risk transmission as the conflict disrupted international trade and commodity supply chains. Stock index futures like CSI 500 also trended significantly downwards, reflecting how geopolitical tensions influence equity market risk sentiment, while trade and supply chain disruptions increased uncertainty in related commodity derivatives.

Stage 5 (2024–2025) witnessed another dramatic change occurred again in the net risk spillover pattern, driven by multiple intertwined factors. The Fed rate cut period (Figure 9)—during which the US shifted its monetary policy towards easing via rate cuts—led to adjustments in global capital flows; for risk assets, changes in liquidity expectations triggered fluctuations in their risk pricing. Varieties like the CSI 500 stock index futures, which are sensitive to capital market liquidity, experienced increased net risk inflow as market participants reassessed risk-return profiles under the new monetary regime. The geopolitical risk and market volatility period (Figure 10)—as events such as the US presidential election and political turbulence in South Korea introduced policy uncertainty and market sentiment shocks—amplified the sensitivity of derivatives (especially stock index futures and commodity futures related to global trade, like iron ore futures) to external news, resulting in pronounced swings in net risk spillover. The US reciprocal tariff implementation period

(Figure 11)—in which the imposition of reciprocal tariffs by the US disrupted international trade relations —impacted the pricing and risk transmission of commodity derivatives (such as cotton futures, which rely on global supply chains) and equity index futures (as trade frictions affect corporate earnings expectations). These events led to a large-scale net risk inflow into affected varieties, positioning them as core 'risk bearers' in the market.

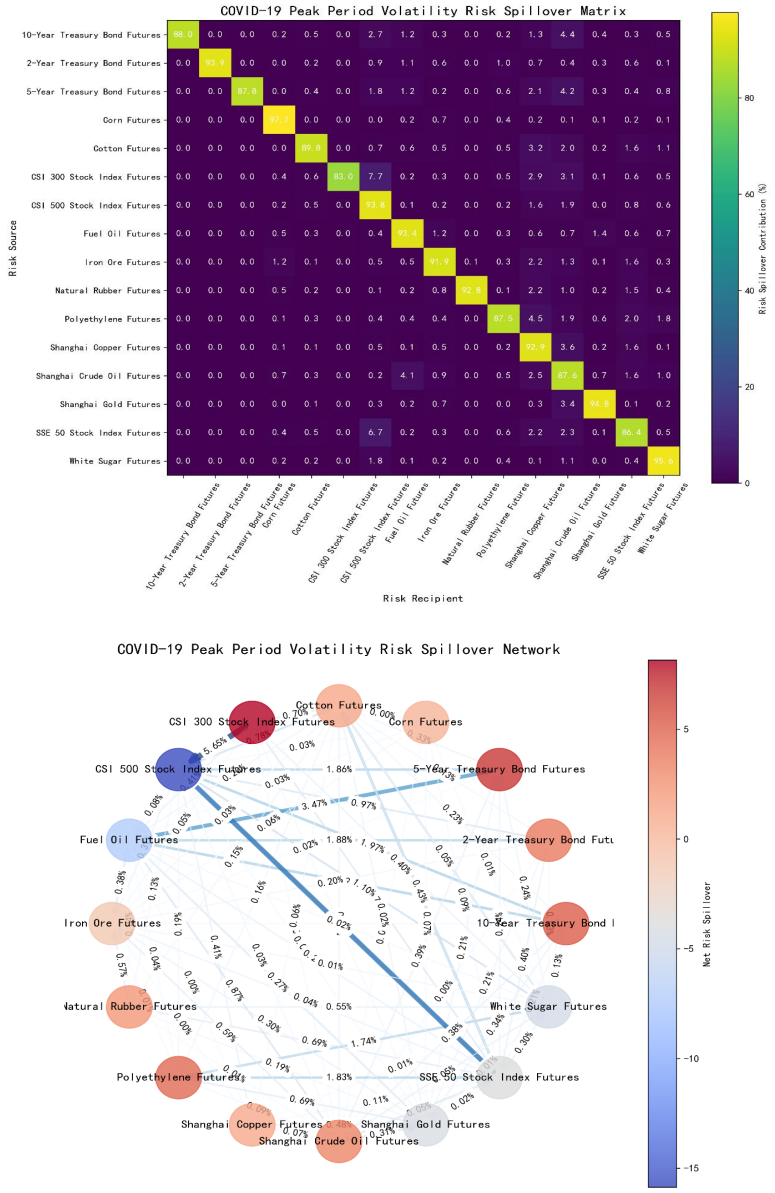

Figure 7. Volatility Risk Spillover Matrix and Network for COVID-19 Peak Period

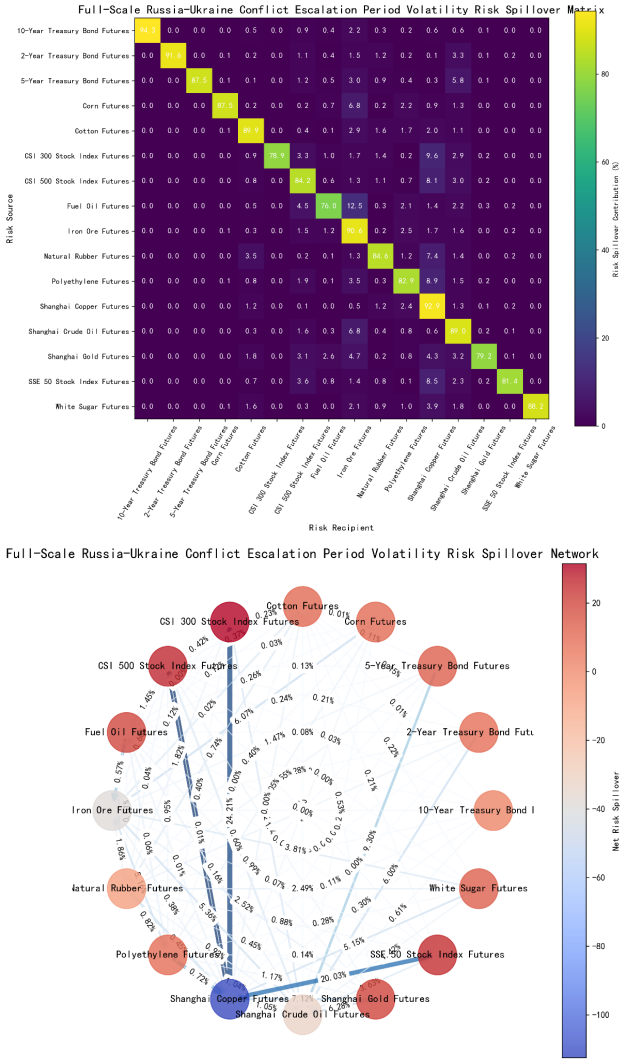

Figure 8. Volatility Risk Spillover Matrix and Network for Full-Scale Russia–Ukraine Conflict Escalation Period

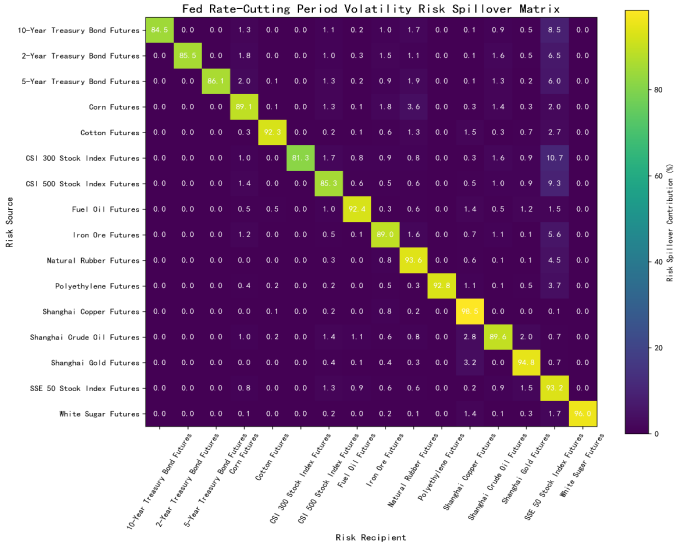

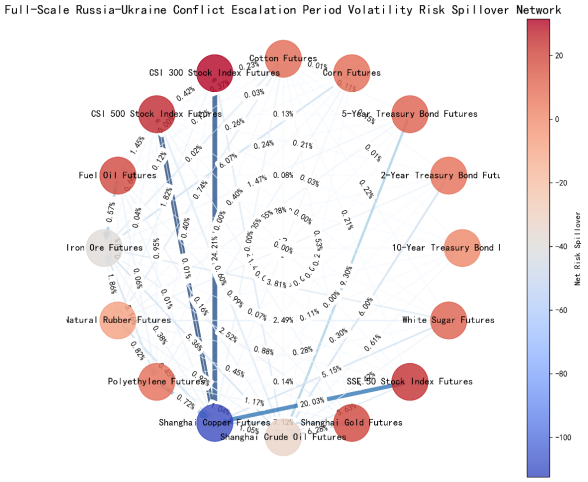

Figure 9. Volatility Risk Spillover Matrix and Network for Fed Rate-Cutting Period

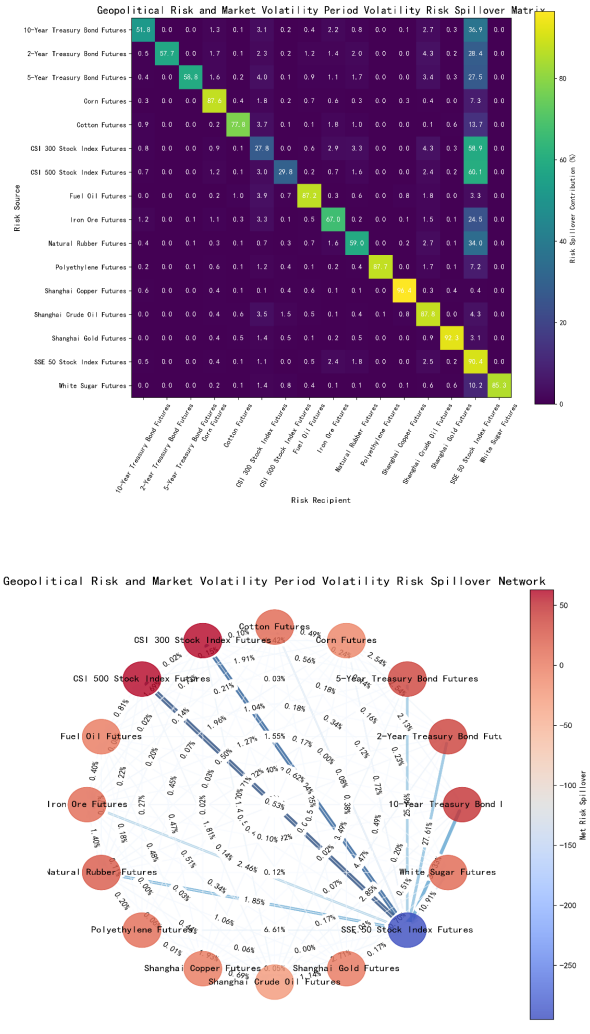

Figure 10. Volatility Risk Spillover Matrix and Network for Geopolitical Risk and Market Volatility Period

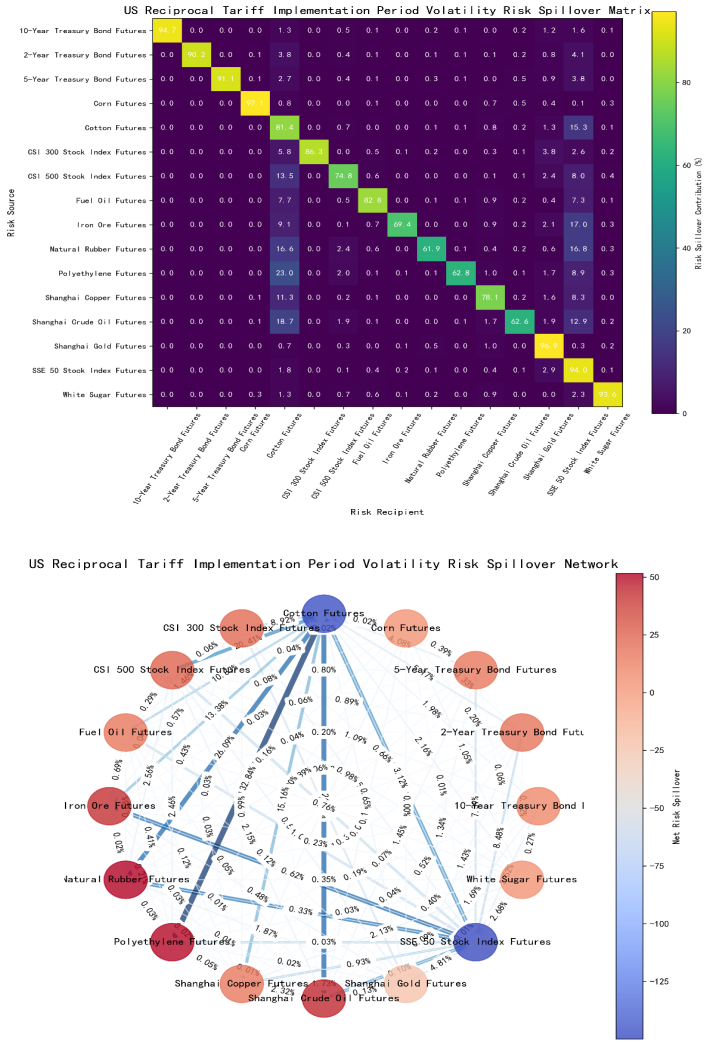

Figure 11. Volatility Risk Spillover Matrix and Network for US Reciprocal Tariff Implementation Period

Notably, different derivative varieties show significant heterogeneity in net risk spillovers, which is closely related to their underlying assets and market attributes, a pattern consistently reflected across all sub-sample figures. Treasury bond futures (10-year, 2-year, and 5-year) remained stable fluctuations near the zero axis throughout the sample period: as ‘safe-haven assets’, have relatively stable pricing logic (driven by macro interest rate policies and liquidity), so the risk transmission of their futures varieties is relatively balanced, and they rarely become the core nodes of net risk inflow or outflow. The net risk spillover of CSI 500 stock index futures fluctuates most drastically, especially during the COVID-19 outbreak in 2020, the Russia–Ukraine conflict in early 2022, and in 2024–2025. Compared with CSI 300 and SSE 50 stock index futures, CSI 500 covers more small- and medium-capitalisation stocks, which are more sensitive to market sentiment and industrial policy changes; therefore, when facing external shocks, the risk spillover of the CSI 500 stock index

futures is more volatile. In contrast, CSI 300 and SSE 50, with a large-cap stock composition, have relatively stable net risk spillover. Among commodity futures, iron ore and cotton futures have extreme net risk spillover performance in the later period. In contrast, crude oil and natural rubber futures remain relatively stable. This difference stems from the characteristics of the industrial chain. The iron ore and cotton industries have relatively concentrated supply-side structures and are highly dependent on downstream demand (such as the real estate and textile industries). When downstream demand changes drastically or supply-side disturbances occur, it can easily cause large-scale risk transmission. The crude oil market, with its globalised trading pattern and sufficient market participants, and the natural rubber industry chain, with its stable supply-demand rhythm, experience smooth risk spillover.

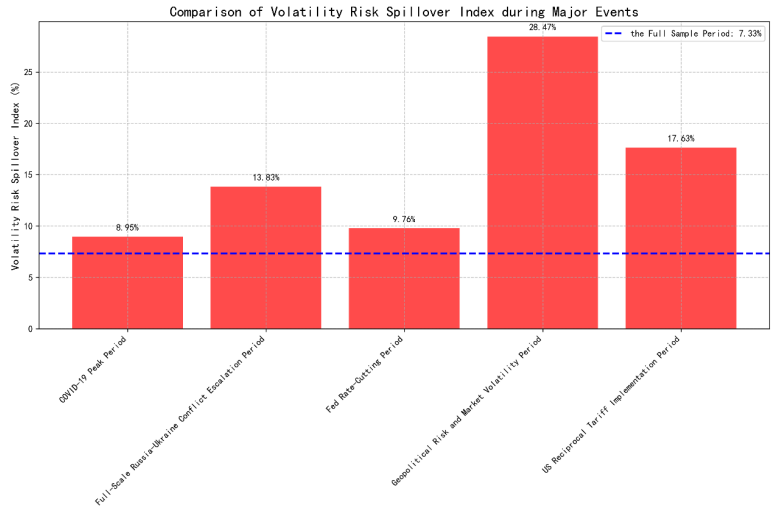

Figure 12. Comparison of Total Volatility Risk Spillover Index across Extreme Events

Network risk spillover index and average strength attained their highest values across all sub-samples during the period of geopolitical risk and market volatility in Figures 12, indicating that under extreme stress scenarios, risk transmits rapidly across nearly all markets. This phenomenon may significantly weaken the effectiveness of portfolio diversification strategies. During the full-scale escalation of the Russia–Ukraine conflict, the bilateral spillover effects between energy and agricultural derivatives increased substantially, highlighting the heterogeneous impact of geopolitical risks on specific commodity sectors.A cross-comparison of the results in Figures 12 and 13 reveals that the structure of the risk transmission network in derivative markets exhibits strong time-varying and asymmetric characteristics. Moreover, its topological properties are critically dependent on the external economic and financial environment.

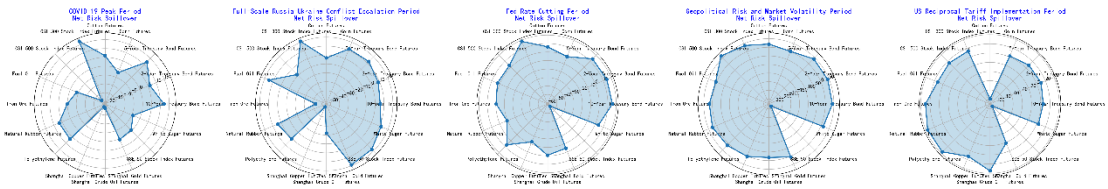

Figure 13. Comparison of Net Risk Spillover Index across Periods of Extreme Events

Model Inputs and Outputs

To comprehensively capture the spatial and temporal characteristics of risk transmission, this study designs a GAT-Transformer fusion model, complemented by an uncertainty-weighted multi-task learning framework, to implement the three-tier early warning system. The Graph Attention Network (GAT) module is dedicated to revealing the spatial topological structure of risk contagion and the asymmetric dependency relationships between markets. Its input includes two core components: the dynamic adjacency matrix of the risk spillover network ($A_t \in R^{N\times N}$, where $N = 16$ corresponding to the number of derivative varieties) and the spatial feature matrix of each node ($X_{node} \in R^{N\times d_n}$). The former is constructed based on the dynamic risk spillover network established in Section 3.1, where each derivative serves as a node and the risk spillover relationships between derivatives are defined as weighted directed edges (with weights corresponding to spillover intensity). The latter is composed of a multi-dimensional feature set based on “trading-technical-risk”, covering three layers: basic trading features (opening price, high price, low price, closing price, trading volume, open interest), technical trend features (price change rate, logarithmic return, volatility, Relative Strength Index (RSI), 10-day/20-day moving averages (MA10/MA20), degree of price deviation from MA20), and risk correlation features (net risk spillover index Net_{it} calculated by Equation (6)). The Transformer module is focused on capturing long-term temporal dependencies and structural breakpoints in cross-market risk transmission. Its input is a temporal feature matrix ($X_{temporal} \in R^{T_{in}\times N\times d_t}$, where $T_{in} = 10$ representing a 10-day historical sequence and $d_t = 14$ corresponding to the 14 types of features in the multi-dimensional feature set).

Notably, as the dynamic risk spillover network in Section 3.1 employs a 100-day rolling window to capture time-varying spillover effects, the network-based feature time series (including adjacency matrices, node spatial features, and temporal sequence features) commences from the 100th sample day. The model adopts a configuration of a rolling step of 1 and a prediction horizon of 1, meaning it utilises the 10-day historical temporal sequence and the current spatial network structure to predict the risk indicators for the next trading

day (i.e., $T_{in}+1$). Finally, an uncertainty-weighted multi-task learning framework is embedded, which adaptively adjusts the loss weight of each task through learnable parameters and establishes thresholds based on the extreme risk distribution. This framework synchronously outputs three core indicators corresponding to the three-tier early warning system: nodal risk, contagion intensity, and systemic vulnerability.

Model Performance Comparison

We designed the training process of the proposed GAT-transformer fusion model to ensure convergence and generalisation. Initially, the dataset was partitioned into training and test subsets in an 8:2 ratio. During model training, we employed the Adam optimiser with an initial learning rate of 1×10^{-3} . Training proceeded for 50 epochs with a batch size of 8. The loss function was constructed as a weighted sum of task-specific losses: node risk loss, contagion intensity loss and system vulnerability loss (Figure 14). Each term targeted the prediction error of the corresponding risk attribute. An uncertainty-aware training mechanism was integrated to bolster robustness against uncertainty. Uncertainty parameters for nodal risk, contagion intensity and system vulnerability (Figure 14) were dynamically learned and incorporated into the loss calculation, thereby balancing the optimisation contribution of each task.

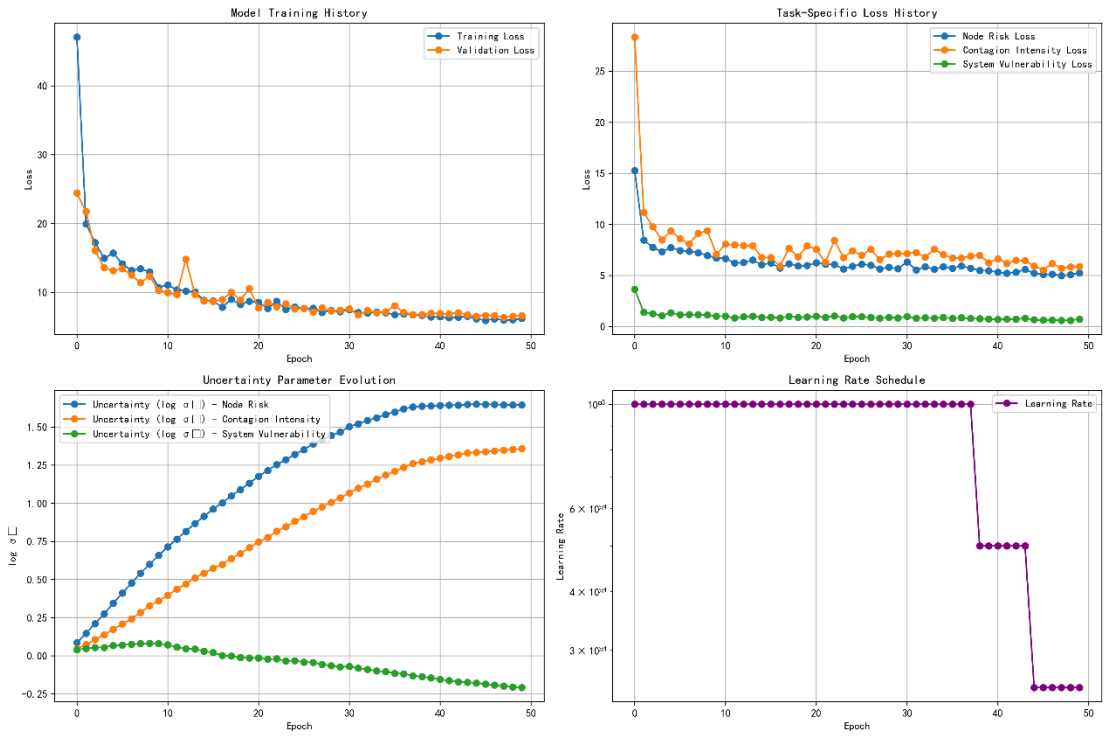

Figure 14. Model Training History and Parameters Evolution

Following training, the model's performance on the held-out test set was comprehensively assessed. For each task (nodal risk, contagion intensity and systemic vulnerability), we computed metrics including MSE, MAE, and the coefficient of determination (R^2) to measure predictive accuracy. Figures 15–17 illustrate the model's efficacy for nodal risk, contagion intensity and system vulnerability, respectively. Scatter points cluster tightly around the diagonal line (indicating strong correspondence between predicted and actual values), while error distributions are centred near zero with narrow variances (reflecting low bias and variability in predictions).

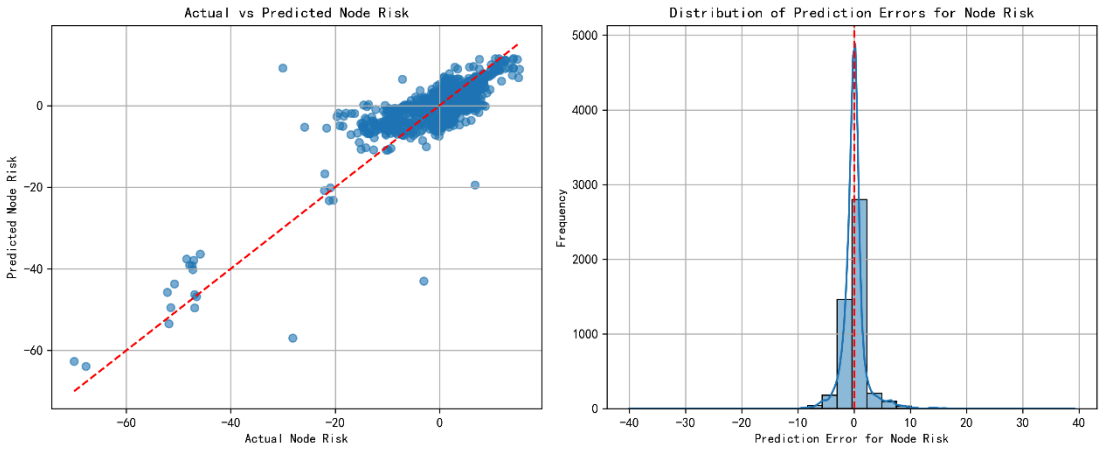

Figure 15. Actual vs. Predicted Scatter Plot and Distribution of Prediction Errors for Nodal Risk

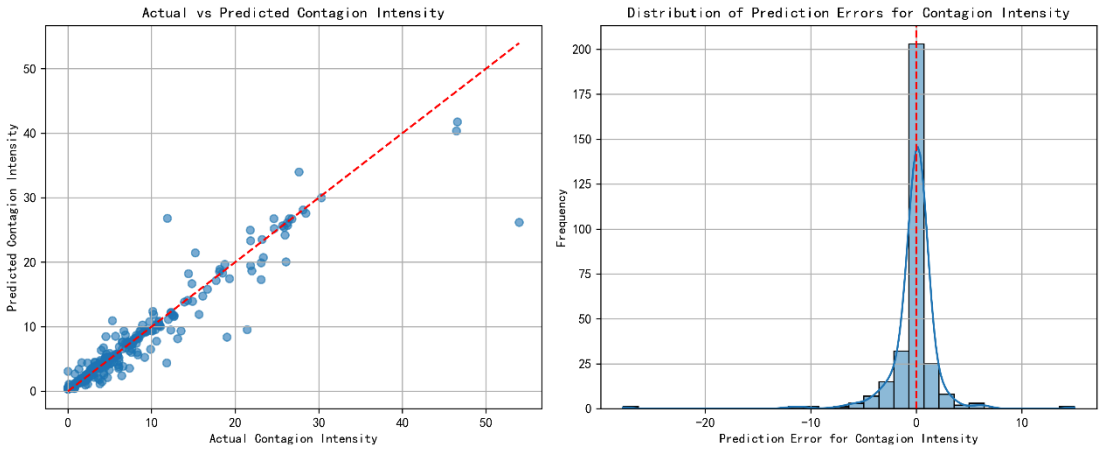

Figure 16. Actual vs. Predicted Scatter Plot and Distribution of Prediction Errors for Contagion Intensity

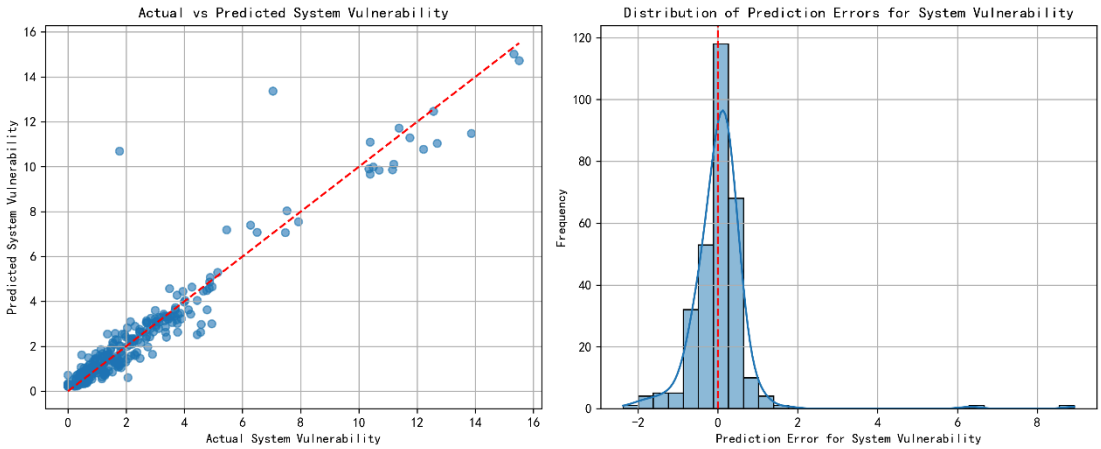

Figure 17. Actual vs. Predicted Scatter Plot and Distribution of Prediction Errors for Systemic Vulnerability

To address the concern regarding potential overfitting and feature redundancy, we conducted an ablation study to systematically evaluate the contribution of each feature group. Specifically, we designed four experimental settings:

Baseline (Model A): Only basic trading features (opening price, high price, low price, closing price, trading volume, open interest) are used as input.

Model B: Adds technical trend features (price change rate, logarithmic return, volatility, RSI, MA10/MA20) to the baseline.

Model C: Adds net risk spillover index (extracted from the Elastic-Net-VAR network) to the baseline.

Model D (Full model): Incorporates both technical trend features and the net risk spillover index simultaneously, which is the complete framework proposed in the manuscript.

All models were trained and evaluated under identical experimental conditions, using the same train/test split and evaluation metrics. The ablation study shows (Table 5) that adding technical trend features consistently improves performance over the baseline, indicating that these indicators provide non-redundant information. Introducing the net risk spillover index yields a further significant boost, confirming its critical role in capturing systemic risk dynamics. The full model (Model D) achieves the best performance, demonstrating that the combination of all feature groups leads to complementary effects rather than overfitting. No performance degradation is observed when adding more features, suggesting that the model does not suffer from feature redundancy.

Table 5. Ablation study results across three risk dimensions

Model	Nodal Risk			Contagion Intensity			Systemic Vulnera-bility		
	MSE	MAE	R^2	MSE	MAE	R^2	MSE	MAE	R^2
Model A	8.421	1.685	0.562	9.573	1.432	0.821	1.124	0.623	0.834
Model B	6.894	1.476	0.641	8.215	1.308	0.863	0.892	0.547	0.873
Model C	6.223	1.389	0.683	7.108	1.197	0.887	0.748	0.496	0.896
Model D	5.639	1.297	0.714	6.136	1.123	0.905	0.664	0.466	0.909

For model performance evaluation, multiple benchmark models were used for comparison, including classical econometric models (VAR, DCC-GARCH and TVP-VAR), unimodal deep learning models (LSTM, Transformer and GAT) and simple feature-concatenation fusion models (GNN-LSTM, TVGCN). Performance was comprehensively evaluated across three prediction tasks—nodal risk, contagion intensity and systemic vulnerability—using metrics such as MSE, MAE and R^2. The empirical results consistently demonstrate (Table 6) that the proposed GAT-transformer fusion model significantly outperforms all benchmark models across all prediction tasks. For example, in the Nodal Risk prediction task, our model's MSE is approximately 15.7% lower than that of the best benchmark model. In predicting the Contagion Intensity, our model achieved an R^2 of 0.905, substantially higher than the DCC-GARCH model (0.621) and the standalone transformer (0.815). Despite the strong performance of TVGCN, our proposed model consistently outperforms it across all three risk dimensions. Compared to TVGCN, our model reduces MSE by approximately 3.2% for Nodal Risk (from 5.824 to 5.639) and by 1.7% for Contagion Intensity (from 6.245 to 6.136). In terms of R^2 for Systemic Vulnerability, our model achieves 0.909, substantially higher than TVGCN's 0.884. The superior performance of our model can be attributed to its ability to simultaneously capture spatial dependencies (via GAT, which learns dynamic cross-market attention weights) and temporal dependencies (via Transformer, which models long-range sequence patterns).This outcome strongly validates the critical importance of simultaneously capturing spatio-temporal dependencies for improving risk prediction accuracy.

Table 6. Comparative Evaluation of Model Prediction Performance

	Nodal Risk			Contagion Intensity			Systemic Vulnera-bility		
	MSE	MAE	R^2	MSE	MAE	R^2	MSE	MAE	R^2
VAR	12.358	2.315	0.412	10.873	1.765	0.487	1.562	0.897	0.523
DCC-GARCH	10.235	2.014	0.502	8.742	1.532	0.621	1.253	0.789	0.654

	Nodal Risk			Contagion Intensity			Systemic Vulnerability		
	MSE	MAE	R^2	MSE	MAE	R^2	MSE	MAE	R^2
TVP-VAR	9.124	1.876	0.546	7.983	1.423	0.647	1.087	0.712	0.705
LSTM	7.854	1.672	0.583	7.231	1.345	0.756	0.987	0.612	0.723
Transformer	6.982	1.453	0.607	6.543	1.214	0.815	0.812	0.543	0.802
GAT	6.215	1.324	0.639	6.872	1.287	0.783	0.756	0.498	0.825
GNN- LSTM	6.012	1.305	0.652	6.321	1.198	0.832	0.712	0.476	0.853
TVGCN	5.824	1.278	0.683	6.245	1.156	0.861	0.689	0.458	0.884
Ours	5.639	1.297	0.714	6.136	1.123	0.905	0.664	0.466	0.909

Network-Based Three-Tier Early Warning Analysis

To assess the early warning performance, prediction outputs for nodal risk, contagion intensity, and systemic vulnerability were transformed into Z-scores, with warning levels (safe, mild warning, moderate warning and severe warning) delineated via predefined Z-score thresholds (Figure 18). The node risk alert time series heatmap exemplifies the model's capacity to discriminate risk across derivative instruments. For instance, treasury bond futures (e.g. 5-year and 10-year treasury bond futures) display more frequent mild to moderate warnings relative to commodity futures (e.g. white sugar futures and Shanghai copper futures), consistent with empirical insights into fixed-income instruments' sensitivity to macroeconomic shocks. Concurrently, the contagion intensity alert and system vulnerability alert time series highlight the model's efficacy in capturing acute risk surges (e.g. early 2020 and late 2024), wherein Z-scores surpass the severe alert threshold—periods corresponding to documented market turmoil.

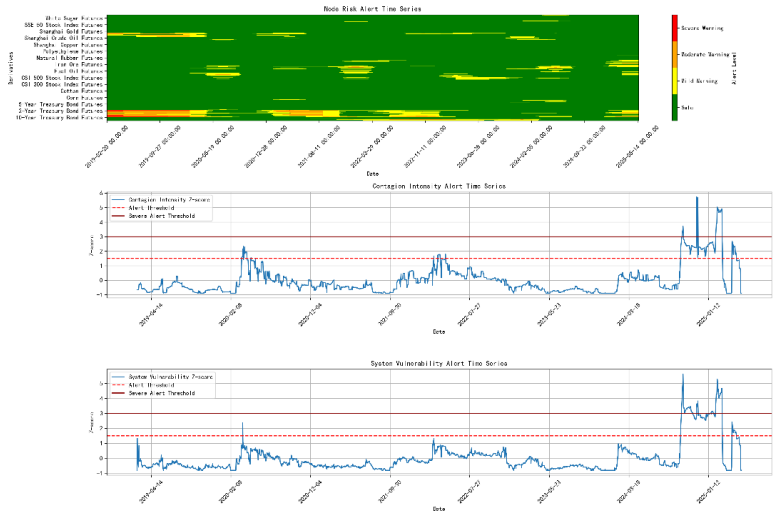

Figure 18. Alert Time Series Plots

Confusion matrices were utilised to quantify classification accuracy across warning levels (Figures 19–21). For nodal risk alert, the matrix records 3,993 true negatives (actual safe and predicted safe). False positives and false negatives are concentrated in adjacent warning tiers (e.g. 153 instances of safe misclassified as mild warning), suggesting the model's conservative bias (erring towards safe) for marginal cases. In contrast, the contagion intensity alert matrix exhibits stronger diagonal dominance (257 accurate safe classifications, 7 true mild warnings, 19 true moderate warnings, and 2 accurate severe warnings), reflecting enhanced precision in discriminating contagion states. The system vulnerability alert matrix demonstrates robust performance, achieving 263 accurate safe classifications and accurately detecting severe vulnerability events (8 accurate severe warnings). The concentration of counts along the diagonal validates the model's reliability in assigning warning levels across all matrices.

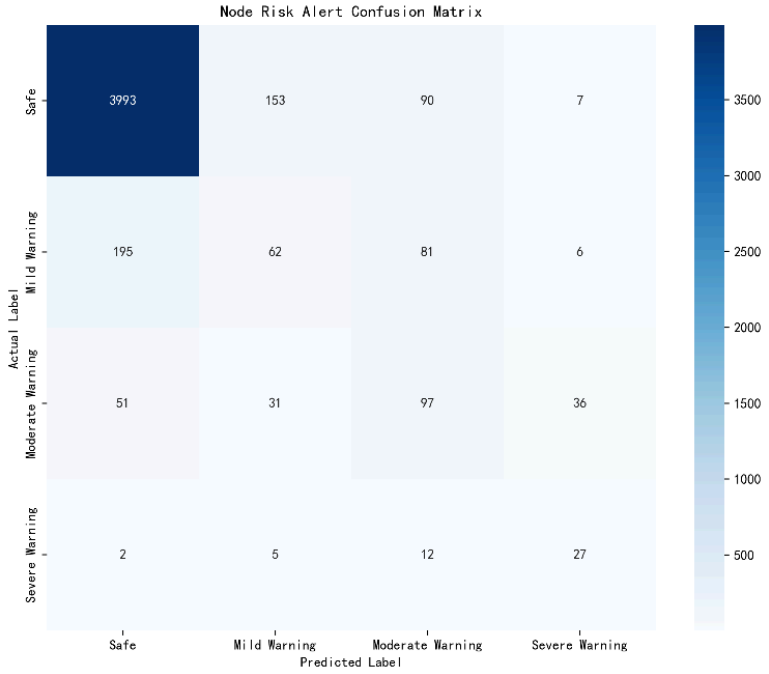

Figure 19. Confusion Matrix for Nodal Risk Alert

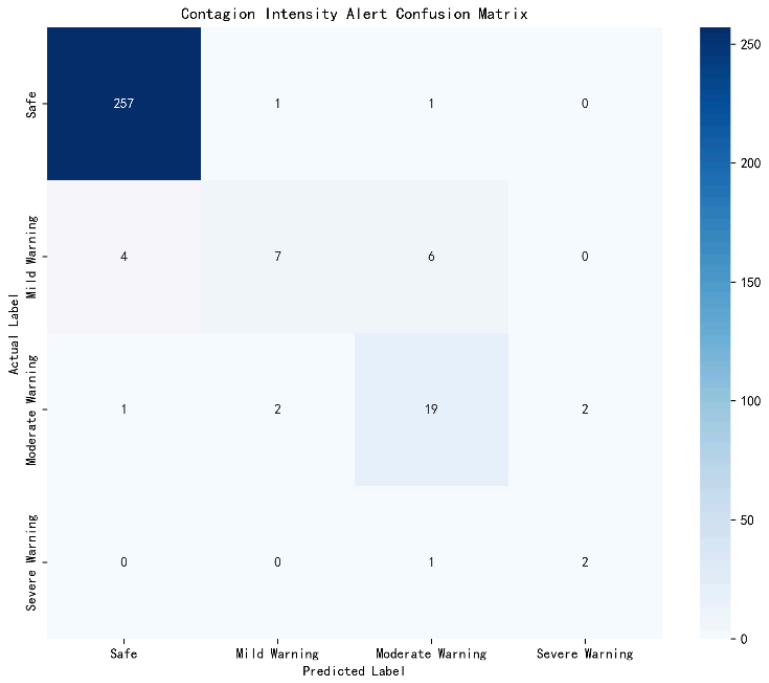

Figure 20. Confusion Matrix for Contagion Intensity Alert

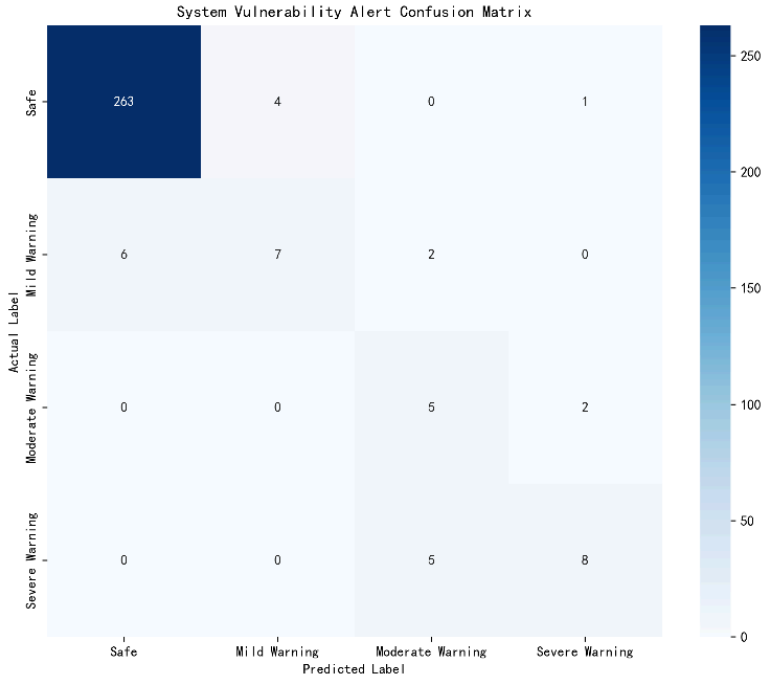

Figure 21. Systemic Vulnerability Alert

Notably, our model also demonstrates significant advantages in the classification performance evaluation for the three-level early warning task (Table 6). We determined warning levels based on the Z-score of the prediction results and computed four classification metrics (accuracy, precision, recall and F1-score) to assess

performance. Results reveal that for the most critical category, systemic vulnerability warning, our model achieved a weighted average F1-score of 0.928 and an accuracy of 0.927, significantly outperforming other comparative models. This finding indicates that our model delivers higher accuracy in continuous value prediction while identifying extreme risk signals more accurately and promptly. Such capabilities hold substantial practical value for regulatory authorities seeking to implement forward-looking risk intervention measures.

Table 7. Comparative Evaluation of Model Early Warning Classification Performance

	VAR	DCC-GARCH	LSTM	Trans-former	GAT	GNN-LSTM	Ours
Nodal Risk							
Accuracy	0.623	0.685	0.752	0.783	0.795	0.821	0.862
Precision	0.615	0.678	0.748	0.779	0.792	0.818	0.862
Recall	0.632	0.691	0.756	0.787	0.801	0.825	0.862
F1-Score	0.623	0.684	0.752	0.783	0.796	0.822	0.861
Contagion Intensity							
Accuracy	0.654	0.723	0.801	0.852	0.863	0.892	0.934
Precision	0.662	0.731	0.810	0.860	0.872	0.901	0.935
Recall	0.648	0.718	0.795	0.847	0.856	0.885	0.934
F1-Score	0.655	0.724	0.802	0.853	0.864	0.893	0.934
Systemic Vulnerability							
Accuracy	0.637	0.702	0.785	0.831	0.846	0.885	0.927
Precision	0.645	0.710	0.792	0.840	0.855	0.892	0.934
Recall	0.632	0.698	0.780	0.827	0.839	0.879	0.927
F1-Score	0.638	0.703	0.786	0.832	0.847	0.885	0.928

To assess the robustness of our early warning outcomes to alternative weight configurations, we conducted a sensitivity analysis by varying the weight on asset-specific risk (ω) from 0.5 to 0.9 in increments of 0.1 (corresponding to market-level risk weights of 0.5 to 0.1). This range encompasses the 0.7 baseline and extends ±20% in both directions. For each weight configuration, we recalculated the Nodal Risk Index for all derivatives across the entire sample period and evaluated the early warning performance using four classification metrics (accuracy, precision, recall and F1-score). The results are summarised in Table A2 (Appendix) and discussed below:

The sensitivity analysis reveals the following key findings: The baseline weight configuration ($\omega = 0.7$) achieves the highest values across four classification metrics, with Accuracy (0.862), Precision (0.862), Recall (0.862), and F1-score (0.861). This confirms that the chosen weight assignment effectively balances

asset-specific and market-level risk contributions for early warning purposes. All alternative weight configurations maintain strong classification performance, with Accuracy ranging from 0.847 to 0.862, and F1-score from 0.844 to 0.861. The maximum deviation from baseline performance is less than 1.8% for Accuracy and 2.0% for F1-score, demonstrating that the early warning system is robust to moderate variations in weight assignment.

CONCLUSION

This study systematically investigates the dynamic risk spillover networks and transmission mechanisms within China's derivative markets, with a specific focus on how volatility in raw fiber futures propagates throughout the textile industrial ecosystem. By mapping these interconnections, the research elucidates the critical pathways through which financial shocks in the textile sector influence broader market stability. We construct a novel GAT-transformer integrated model, revealing that the risk spillover network structure of derivative markets exhibits pronounced time-varying and asymmetric characteristics. Moreover, its total spillover index intensifies sharply during extreme events, such as the COVID-19 pandemic and geopolitical conflicts, leading to notable risk resonance effects. The proposed GAT-transformer architecture can simultaneously capture spatio-temporal dependencies in risk propagation and significantly outperform traditional econometric models and unimodal deep learning benchmarks across three critical tasks: nodal risk prediction, contagion intensity measurement and systemic vulnerability assessment. This finding demonstrates the substantial potential of sophisticated AI models in financial risk management. Our empirical analysis successfully identifies systemically important derivatives—such as the CSI 300 stock index futures and crude oil futures—and elucidates the key pathways through which risks propagate across the network, thereby revealing the intrinsic mechanisms of cross-market risk transmission. Furthermore, the multi-task learning framework underpins a three-tier early warning mechanism targeting nodal risk, contagion intensity, and systemic vulnerability. This framework provides a scientific and quantitative basis for precise and differentiated risk prevention and control.

Based on these conclusions, this study proposes the following policy recommendations.

Financial regulatory authorities should prioritise establishing an intelligent risk monitoring platform that incorporates such AI models. Such a platform would enable real-time visualisation and dynamic early warning of risk spillovers in derivative markets, shifting the paradigm from passive response to proactive intervention. Regulatory focus should concentrate on those derivatives identified as 'net risk transmitters' considering their systemic importance. Their anomalous trading behaviours should be subjected to intensified monitoring, and

targeted stress tests should be conducted regularly to determine their risk-bearing and diffusion capacities under extreme scenarios. More importantly, moving beyond traditional institutional and segmented supervision models is essential. For example, a cross-market, cross-industry joint risk prevention and control mechanism should be established. Detailed contingency plans must be preemptively formulated and tailored to the critical risk transmission pathways revealed by the empirical analysis. This approach would allow for swift and precise disruption of contagion chains when risks materialise, preventing localised risks from escalating into systemic crises.

Furthermore, this study's findings offer crucial practical guidance for market participants, including financial institutions, investment funds, and industrial firms. Such firms should incorporate risk spillover network analytics into their internal risk management systems. Utilising the model's risk forecasts and early warnings can help with dynamic portfolio optimisation, proactively avoid high-risk contagion paths, and enhance portfolio resilience. Simultaneously, investors should monitor changes in the topology of the risk network and use this information as a key input for formulating macro-hedging strategies. For example, during periods of sharply elevated network connectivity and heightened systemic risk, it would be prudent to significantly reduce risk asset allocation and increase safe-haven assets. Conversely, when specific instruments are identified as risk transmission hubs, corresponding hedging operations can be employed to manage potential exposures.

Despite the contributions of this study, several limitations remain, pointing to directions for future research. First, while this study primarily constructs the risk network based on trading price and volume data, future research could incorporate news sentiment, social media mood, macroeconomic indicators, and even alternative data to create a richer heterogeneous information network, thereby more comprehensively capturing the multi-dimensional factors influencing risk transmission. Second, the current risk spillover network relies on spillover matrices pre-calculated via econometric models. Future research could explore fully data-driven dynamic GNNs to identify network structures and simultaneously extract node features within a unified end-to-end framework, further enhancing the model's adaptive capabilities. Finally, the proposed framework can be extended to emerging markets, such as cryptocurrencies and green finance derivatives, to validate its universality and robustness across different market structures and data frequencies. This approach continuously provides cutting-edge intelligent decision support for the stable operation of the textile industrial economy and the adequate supervision of its associated financial markets. By synchronising predictive analytics with

raw fiber price fluctuations, the system ensures that the textile sector remains anchored against systemic risks in the broader derivative landscape.

Author Contributions

Conceptualization –Pengbo Zhang and JinboPan; methodology – Pengbo Zhang and JinboPan; investigation – Pengbo Zhang and JinboPan; writing-original draft preparation – Pengbo Zhang and JinboPan. All authors have read and agreed to the published version of the manuscript.

Conflicts of Interest

The authors declare no conflict of interest.

Funding

This research received no external funding.

Acknowledgements

Not applicable.

REFERENCES

[1] Diebold FX, Yilmaz K. Measuring financial asset return and volatility spillovers, with application to global equity markets. The Economic Journal. 2009; 119(534):158-171. doi: 10.1111/j.1468-0297.2008.02208.x

[2] Hammoudeh S, McAleer M. Risk management and financial derivatives: An overview. The North American Journal of Economics and Finance. 2013; 25:109-115. doi: 10.1016/j.najef.2012.06.014

[3] Mensi W, Hammoudeh S, Reboredo JC, Yoon SM. Dynamic spillovers among major energy and cereal commodity prices. Energy Economics. 2014; 43:225-243. doi: 10.1016/j.eneco.2014.03.004

[4] Kang SH, McIver R, Yoon SM. Dynamic spillover effects among crude oil, precious metal, and agricultural commodity futures markets. Energy Economics. 2017; 62:19-32. doi: 10.1016/j.eneco.2016.12.011

[5] Wang QW, Dai XY, Zhou DQ. Dynamic Correlation and Risk Contagion Between "Black" Futures in China: A Multi-scale Variational Mode Decomposition Approach. Computational Economics. 2020; 55(4):1117-1150. doi: 10.1007/s10614-018-9857-y

[6] Dahl RE, Oglend A, Yahya M. Dynamics of volatility spillover in commodity markets: Linking crude oil to agriculture. Journal of Commodity Markets. 2020; 20:100111. doi: 10.1016/j.jcomm.2019.100111

[7] Moratis G. Quantifying the spillover effect in the cryptocurrency market. Finance Research Letters. 2021; 38:101534. doi: 10.1016/j.frl.2020.101534

[8] Diebold FX, Yilmaz K. On the network topology of variance decompositions: Measuring the connectedness of financial firms. Journal of Econometrics. 2014; 182(1):119-134. doi: 10.1016/j.jeconom.2014.04.012

[9] Demirer M, Diebold FX, Liu L, Yilmaz K. Estimating global bank network connectedness. Journal of Applied Econometrics. 2018; 33(1):1-15. doi: 10.1002/jae.2585

[10] Gao Y, Li YY, Wang YJ. Risk spillover and network connectedness analysis of China's green bond and financial markets: Evidence from financial events of 2015-2020. The North American Journal of Economics and Finance. 2021; 57:101386. doi: 10.1016/j.najef.2021.101386

[11] Laborda R, Olmo J. Volatility spillover between economic sectors in financial crisis prediction: Evidence spanning the great financial crisis and Covid-19 pandemic. Research in International Business and Finance. 2021; 57:101402. doi: 10.1016/j.ribaf.2021.101402

[12] Gong X, Liu Y, Wang X. Dynamic volatility spillovers across oil and natural gas futures markets based on a time-varying spillover method. International Review of Financial Analysis. 2021; 76:101790. doi: 10.1016/j.irfa.2021.101790

[13] Dai ZF, Zhu HY. Time-varying spillover effects and investment strategies between WTI crude oil, natural gas and Chinese stock markets related to belt and road initiative. Energy Economics. 2022; 108:105883. doi: 10.1016/j.eneco.2022.105883

[14] Yang Z, Chen Y, Xie R. Research on systemic risk measures and cross-sector risk spillover effect of financial institutions in China. Journal of Financial Research. 2018; (10):19-37.(in Chinese)

[15] Gong X, Xiong X. A study of financial risk contagion from the volatility spillover network perspective. Journal of Financial Research. 2020; (5): 39-58. (in Chinese)

[16] Iqbal N, Bouri E, Roubaud D. Modelling extreme risk spillovers in the commodity markets around crisis periods including COVID19. Annals of Operations Research. 2023; 330(1-2):305-334. doi: 10.1007/s10479-022-04522-9

[17] Naeem MA, Hamouda F, Karim S. Tail risk spillover effects in commodity markets: A comparative study of crisis periods. Journal of Commodity Markets. 2024; 33:100370. doi: 10.1016/j.jcomm.2023.100370

[18] Gnagne PX, Simo-Kengne BD, Manguzvane MM. The spillover and contagion effects of sovereign risk on stock markets. Economic Modelling. 2024; 141:106921. doi: 10.1016/j.econmod.2024.106921

[19] Zhou W, Guo J, Lu S. Key market identification, mechanism transmission, and extreme shock during the risk spillover process: an empirical study of the G20 FOREX markets. Empirical Economics. 2023; 65(6):2549-2582. doi: 10.1007/s00181-023-02436-4

[20] Xia ML, Chen ZH, Wang P. Dynamic Risk Spillover Effect between the Carbon and Stock Markets under the Shocks from Exogenous Events. Energies. 2023; 16(1):97. doi: 10.3390/en16010097

[21] Liu X, Zhou D, Zhang Y. Research on dynamic network spillover of extreme risks in financial markets and identification of high risk. Management World. 2025; 41(5):15-38. (in Chinese) doi: 10.19744/j.cnki.11-1235/f.2025.0069

[22] Dong F, Li Z, Wang S, Huang Z. Research on risk spillover effects between geopolitical risk and energy, foreign exchange, and gold markets. Systems Engineering - Theory & Practice. 2025; 46(01):141-157. (in Chinese).Available from: https://link.cnki.net/urlid/11.2267.N.20250217.1117.009

[23] Ren X, Xiao S, Sun X. Tail risk spillover of commodity futures markets. Accounting and Finance. 2025; 65(1):109-141. doi: 10.1111/acfi.13321

[24] Sahiner M. Volatility Spillovers and Contagion During Major Crises: An Early Warning Approach Based on a Deep Learning Model. Computational Economics. 2024; 63(6):2435-2499. doi: 10.1007/s10614-023-10412-4

[25] Tang P, Xu W, Wang HS. Network-Based prediction of financial cross-sector risk spillover in China: A deep learning approach. The North American Journal of Economics and Finance. 2024; 72:102151. doi: 10.1016/j.najef.2024.102151

[26] Rizvi SKA, Naqvi B, Mirza N. Is green investment different from grey? Return and volatility spillovers between green and grey energy ETFs. Annals of Operations Research. 2022; 313(1):495-524. doi: 10.1007/s10479-021-04367-8

[27] Tiwari AK, Abakah EJA, Lee CC. Quantile risk spillovers between energy and agricultural commodity markets: Evidence from pre and during COVID-19 outbreak. Energy Economics. 2022; 113:106235. doi: 10.1016/j.eneco.2022.106235

[28] Chen C, Chen W, Shang L. et al. Price discovery and volatility spillovers in the interest rate derivatives market. Humanities & Social Sciences Communications. 2024; 11:360. doi: 10.1057/s41599-024-02788-x

[29] Luo CQ, Qu Y, Dong L. Risk spillover from international crude oil markets to China's financial markets: Evidence from extreme events and US monetary policy. The North American Journal of Economics and Finance. 2024; 70:102041. doi: 10.1016/j.najef.2023.102041

[30] Shi K, Gong JL. The influence of the spillover between futures and spot markets on hedging policy: evidence from Chinese stock markets. Frontiers in Physics. 2023; 11:1293182. doi: 10.3389/fphy.2023.1293182

[31] Lu CY, Teng ZQ, Fang YT. Analysis of Early Warning of RMB Exchange Rate Fluctuation and Value at Risk Measurement Based on Deep Learning. Computational Economics. 2022; 59(4):1501-1524. doi: 10.1007/s10614-021-10172-z

[32] Rayadurgam VC, Mangalagiri J. Does inclusion of GARCH variance in deep learning models improve financial contagion prediction? Finance Research Letters. 2023; 54:103707. doi: 10.1016/j.frl.2023.103707

[33] Deng YX, Fang GB, Ma HM. Dynamic Connectedness Among Oil, Food Commodity, and Renewable Energy Markets: Novel Perspective from Quantile Dependence and Deep Learning. Journal of the Knowledge Economy. 2024; 15:9935-9947. doi: 10.1007/s13132-023-01485-5

[34] Yang JJ, Gong XG, Fang AC. Extreme Risk Spillover from Commodity Markets to Green Finance Markets: New Evidence Utilizing GAN and GARCH Model. Computational Economics. 2025. doi: 10.1007/s10614-025-11004-0

[35] Veličković P, Cucurull G, Casanova A, Romero A, Liò P, Bengio Y. Graph Attention Networks. International Conference on Learning Representations. 2018. doi: 10.48550/arXiv.1710.10903

[36] Rahmani S, Baghbani A, Bouillard P, Patterson Z. Graph Neural Networks for Intelligent Transportation Systems: A Survey. IEEE Transactions on Intelligent Transportation Systems. 2023; 24(8):8846-8885. doi: 10.1109/TITS.2023.3257759

[37] Khemani B, Patil S, Tanwar S. A review of graph neural networks: concepts, architectures, techniques, challenges, datasets, applications, and future directions. Journal of Big Data. 2024; 11(1):18. doi: 10.1186/s40537-023-00876-4

[38] Song Y, Du H, Shi H. Research on Financial Risk Intelligent Monitoring and Early Warning Model Based on LSTM, Transformer, and Deep Learning. Journal of Organizational and End User Computing. 2024; 36(1):1-24. doi: 10.4018/JOEUC.337607

[39] Ren Y, Jiang J, Ni Q. A study on financial crisis early warning based on graph neural networks models:A perspective of information spillover among industries. Statistical Research. 2022; 39(8):141-160. (in Chinese) doi: 10.19343/j.cnki.11-1302/c.2022.08.010

APPENDIX

Table A1. CUSUM Test Statistics for Parameter Stability

Event Window	Date / Period	CUSUM Statistic	5% Critical Bound	CUSUM of Squares Statistic	5% Critical Bound
COVID-19 pandemic	Feb 2020	1.287	±1.524	0.146	±0.140
	Mar 2020	1.198	±1.526	0.112	±0.140
Russia–Ukraine conflict	Feb 2022	1.342	±1.531	0.138	±0.141
	Mar 2022	1.156	±1.533	0.098	±0.141
Fed rate-cutting cycle	Sep 2024	1.104	±1.537	0.084	±0.142
	Oct 2024	1.276	±1.538	0.089	±0.142
Election political cycles	Nov 2024	1.398	±1.539	0.137	±0.142
	Dec 2024	1.223	±1.540	0.107	±0.142
US reciprocal tariffs	Apr 2025	1.351	±1.542	0.141	±0.143
	May 2025	1.198	±1.543	0.098	±0.143

Note: Critical bounds are calculated at the 5% significance level. Transient exceedances are short-lived (lasting no more than one month) and do not persist beyond the rolling window length of 100 days.

Table A2. Sensitivity Analysis of Nodal Risk Index Weighting

Weight (ω)	Market Weight ($1-\omega$)	Accuracy	Precision	Recall	F1-score
0.5	0.5	0.847	0.851	0.838	0.844
0.6	0.4	0.856	0.859	0.852	0.855
0.7	0.3	0.862	0.862	0.862	0.861
0.8	0.2	0.858	0.860	0.855	0.857
0.9	0.1	0.849	0.852	0.843	0.847

Note: All values represent averages across the full sample period and five major event windows.